ISSN 1882-3432

TECHNOLOGY DEVELOPMENT CENTER NEWS

NATIONAL INSTITUTE OF INFORMATION AND COMMUNICATIONS TECHNOLOGY

Serial No. 36 November 2016

CONTENTS

Proceedings of the 15th NICT TDC Symposium (Kashima, June 30, 2016)

Detection of TEC Anomalies by Using Correlation Analysis -2011 Tohoku-Oki case-

Takuya Iwata
(*iwata.takuya.37m@st.kyoto-u.ac.jp*),
Ken Umeno , *Department of Applied*

Mathematics and Physics, Graduate school of Informatics, Kyoto University,
Yoshidahon-machi, Sakyo-ku, Kyoto, Japan

Abstract: Ionosphere contains large amount of electrons and signals sent by GPS (Global Positioning System) and other GNSS (Global Navigation Satellite System) satellites are affected by these electrons. We can observe daily changes of Total Electron Content (TEC) in ionosphere by using the phase differences between the two carrier waves from GNSS satellites. In recent research, some papers show the presence of the preseismic TEC anomalies which can be seen before large earthquakes in the world [2, 3, 4]. However, these analysis methods have some problems which cause arguments among the related researchers [5, 6, 7]. In this research, we propose an analysis method which can detect TEC anomalies before large earthquakes. Our method adopted the correlation analysis (also used in VLBI analysis) to reduce noises on TEC data. As a result, our proposed method detected TEC anomalies about one hour before 2011 Tohoku-Oki earthquake, which is the largest earthquake in Japan during recent years. As further research, we will check other large earthquakes and establish a robust method to detect TEC anomalies before earthquakes.

1. Introduction

Japan has a dense GNSS observation network (GNSS Earth Observation NETwork, GEONET) to correct and analyze the large amount of GNSS observation data. These GNSS data (in recent a few years) are open to public and anyone can download and analyze freely via the Internet(terras.gsi.go.jp).

TEC data analysis is one of the major researches using GNSS. In particular, analyzing TEC data before large earthquakes has been drawn considerable attention.

In this research, we analyzed TEC data before the 2011 Tohoku-Oki earthquake data, which is also freely available from GEONET.

2. Analysis method

STEP 0. Choose the central GNSS station and set up three parameters, i.e. t_{sample}, t_{test}, and M. t_{sample} is the length of data used for regression *training* and t_{test} is the length of data used for regression *test*, and the value M denotes the number of GNSS stations we use.
STEP 1. At each station i and at each time epoch t, let $SampleData$ be the data from t to $t+t_{sample}$ and $TestData$ be the data from $t+t_{sample}$ to $t+t_{sample}+t_{test}$.
STEP 2. Fit a curve to $SampleData$ by the least square method.
STEP 3. Calculate a deviation of the $TestData$ from the model curve, representing as an "anomaly". The anomaly at station i at time t' is denoted as $x_{i,t'}$.
STEP 4. Calculate a summation of correlations between the anomalies at the central GNSS station and the surrounding stations as follows:

$$C(T) = \frac{1}{N \times M} \sum_{i=1}^{M} \sum_{j=0}^{N-1} x_{i,t+t_{sample}+j\Delta t} x_{0,t+t_{sample}+j\Delta t} \tag{1}$$

$$T = t + t_{sample} + t_{test}$$

Here, N is the number of data in *TestData*, Δt is a sampling interval in *TestData*, which means $\Delta t = t_{test}/(N-1)$, and $i = 0$ means the central GNSS station, where $t_{sample} = 2.0$ [hours], $t_{test} = 0.25$ [hours] and $M = 30$ [stations].

We can choose arbitrary functions as a fitting curve in STEP 2. In this research, we adopted 7th polynomial functions.

3. 2011 Tohoku-Oki earthquake

The 2011 March 11 (05:46 UT) Tohoku-Oki earthquake occurred at the northeast Japan. Its magnitude is huge (Mw 9.0) and the earthquake caused great damage to this area and all over Japan. This earthquake is the largest earthquake during the period that the GNSS data are freely available from GEONET.

Figure 1 shows the location of the epicenter and the SIP (Sub Ionospheric Point) track of the 26 GPS satellite and the 0214 (Kitaibaraki) GNSS receiver. The intersection of the line-of-sight and ionosphere is called as IPP (Ionospheric Pierce Point) and SIP is its projection to the ground.

4. Results

Figure 2 shows the result of the correlation analysis on March 11, 2011. We chose the GPS satellite

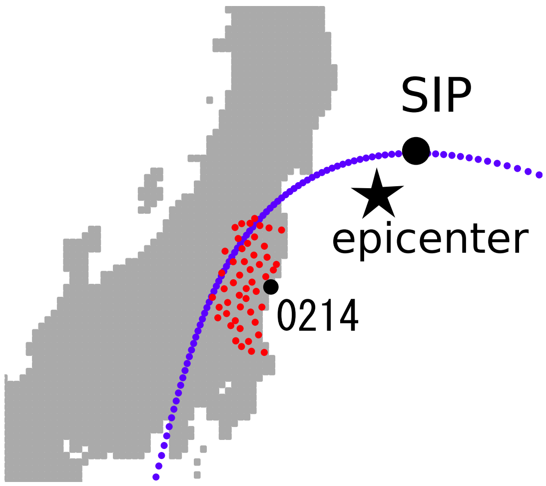

Figure 1. The location of the epicenter of the 2011 Tohoku-Oki earthquake and the SIP track of the GPS satellite 26 and the 0214 receiver. The bold black circle indicates the location of SIP when the earthquake occured.

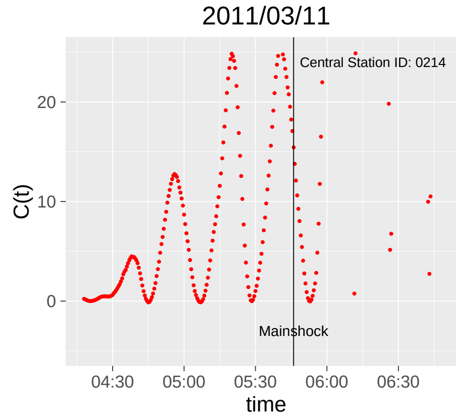

Figure 2. The result of correlation analysis on the March 11, 2011. We used the TEC data derived from the pair of the GPS satellite 26 and the 0214 GNSS station (and 30 stations surrounding it) to calculate correlation values. The x-axis is time (UT) and the y-axis is the correlation values defined in eq. (1). The black vertical line is the earthquake occurrence time (05:46 UT).

26 and the 0214 (Kitaibaraki) station as a center station. The x-axis is time (UT) and the y-axis is the correlation values defined in eq. (1). The black vertical line in the figure shows the earthquake occurrence time (05:46 UT). As time approaches the earthquake occurrence time, the correlation value (C(t)) is becoming large. Furthermore, the correlation value looks the characteristic wave-like pattern.

Figure 3 shows the results of the correlation analysis on non-earthquake days, namely, 10 days, 20days, 30days and 40 days before the earthquake. Comparing Fig. 2 with Fig. 3, we can confirm that the correlation values on the earthquake day are much larger than that on the non-earthquake days. The correlation values on non-earthquake days are at most 5, however, the correlation values on earthquake day are over 20 before the earthquake.

Figure 4 shows the results of the correlation analysis of all the GNSS stations in GEONET before the main shock. The red area in the figure means the TEC-anomalous region and the yellow area means the clam (not anomalous) region. The anomalous area can be seen near the epicenter as the earthquake occurrence time (05:46 UT) is closing.

While the physical mechanisms responsible for the TEC anomalies before the earthquake are not so clear up to now, some physical models which explain it have been proposed. One of the models is based on the laboratory experimental results of stressed rock [8, 9]. According to the experimental results, as rock are subject to stress, they produce positive holes at the surface of the rock. Hence, the electric fields are generated in the air and affect the ionosphere. A lithosphere-atmosphere-ionosphere coupling model based on the experimental results is proposed and improved in recent studies [10, 11]. This model can explain the mechanisms of TEC anomalies before large earthquakes [12].

5. Summary

In this research, we proposed the correlation analysis for detecting TEC anomalies. This analysis method is familiar to Informatics and radio astronomy, but has not been applied to analyzing TEC data. In the 2011 Tohoku-Oki earthquake case, the TEC anomaly near the epicenter is detected about one hour before the main shock by the correlation analysis. This anomalous TEC values have a characteristic pattern, but the physical mechanism responsible for it is still unclear. As further research, other large earthquakes should be investigated to confirm the presence of TEC anomalies before large earthquakes. Furthermore, it is anticipated that the physical mechanisms which reveal the relationship between the seismic activities and ionospheric disturbances are explored.

References

[1] Iwata, T. and K. Umeno, Correlation analysis for pre-seismic total electron content anomalies around the 2011 Tohoku-Oki earth-

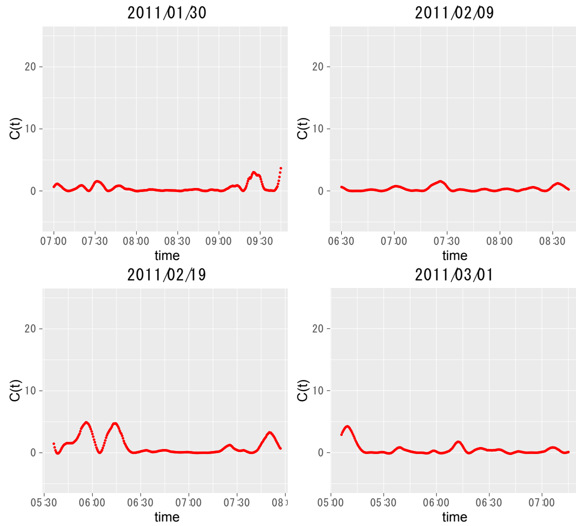

Figure 3. The results of correlation analysis on non-earthquake days (10 days, 20 days, 30 days and 40 days before the earthquake). We used same the GPS satellite and the GNSS stations as Fig. 2.

quake, J. Geophys. Res. Space Phys., 121, doi: 10.1002/2016JA023036., 2016.

[2] Heki, K., Ionospheric electron enhancement preceding the 2011 Tohoku-Oki earthquake, Geophys. Res. Lett., Vol. 38, L17312, 2011.

[3] Heki, K. and Y. Enomoto, Preseismic ionospheric electron enhancements revisited, J. Geophys. Res. Space Phys., vol. 118, pp. 6618–6626, 2013.

[4] Heki, K. and Y. Enomoto, Mw dependence of preseismic ionospheric electron enhancements, J. Geophys. Res. Space Phys., vol. 120, pp. 7006–7020, 2015.

[5] Kamogawa, M. and Y. kakinami, Is an ionospheric electron enhancement preceding the 2011 Tohoku-oki earthquake a precursor?, J. Geophys. Res. Space Phys., vol. 118, No. 4, pp. 1751–1754, 2011.

[6] Utada, H. and H. Shimizu, Comment on 'Preseismic ionospheric electron enhancements revisited' by K. Heki and Y. Enomoto, J. Geophys. Res. Space Phys., vol. 119, no. 7, pp. 6011–6015, 2011.

[7] Maci, F., J. N. Thomas, F. Villani, J. A. Secan and N. Rivera, On the onset of ionospheric precursors 40 min before strong earthquakes, J. Geophys. Res. Space Phys., vol. 120, No. 2, pp. 1383–1393, 2015.

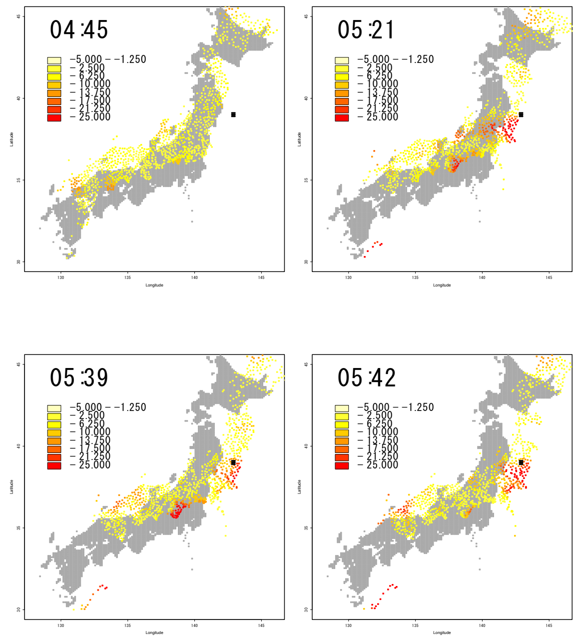

Figure 4. The results of correlation analysis of all the GNSS stations in Japan on the earthquake day. We used same the GPS satellite 26. The black sign is the epicenter. The earthquake occurrence time is 05:46 [UT].

[8] Freund, F., Toward a unified solid state theory for pre-earthquake signals, Acta Geophys., vol. 58, No. 5, pp. 719–866, 2010.

[9] Freund, F., Earthquake forewarning – A multidisciplinary challenge from the ground up to space, Acta Geophys., vol. 61, No. 4, pp. 775–807, 2013.

[10] Kuo, C. L., J. D. Huba, G. Joyce and L. C. Lee, Ionosphere plasma bubbles and density variations induced by pre-earthquake rock currents and associated surface charges, J. Geophys. Res., vol. 116, A10317, 2011.

[11] Kuo, C. L., L. C. Lee and J. D. Huba, An improved coupling model for the lithosphere-atmosphere-ionosphere system, J. Geophys. Res. Space Phys., vol. 119, pp. 3189–3205, 2014.

[12] Kuo, C. L., L. C. Lee and K. Heki, Preseismic TEC changes for Tohoku-Oki earthquake: Comparisons between simulations and observations, Terr. Atmos. Ocean. Sci., vol. 26, pp. 63–72, 2015.

Water Vapor Radiometer: Challenge Again

Noriyuki Kawaguchi (*kawagu.nori@nao.ac.jp*),

Visiting Professor, Shanghai Observatory
Professor Emeritus, National Astronomical Observatory,
Eldia 1507, 1-29-1 Tamagawa, Chofu, Tokyo, 182-0025 Japan

Abstract: In 1984, a VLBI group in Kashima Branch, Radio Research laboratory (at present Kashima Space Technology Center of NICT, National Institute of Information and Communications Technology) tried to develop a water vapor radiometer, WVR, which aims at obtaining better accuracy in geodetic VLBI observations. With the WVR data they did not get remarkable improvements on geodetic solutions for the US-Japan joint VLBI program. Since then the development of WVR has been inactive in Japan until the KEK, High Energy Accelerator Research Organization in Japan) succeeded to measure the wideband spectrum of a resonance pattern of a water vapor molecule in the atmosphere in 2015. The success inspires developments of a new advanced WVR in Japan.

Here I will review the current state of developments on the WVR in the world and give suggestions on the new WVR in future.

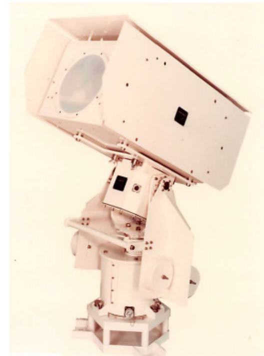

Figure 1. K3 WVR developed by Kashima in the first trial

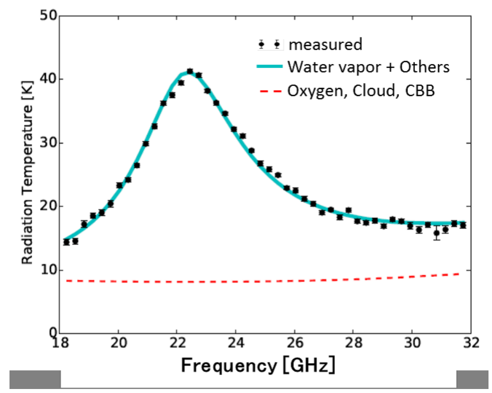

Figure 2. Wideband water vapor emission spectrum detected by KEK WVR

1. Introduction

In 1985 a Water Vapor Radiometer, WVR, was developed by a VLBI group in Kashima Branch, Radio Research laboratory (at present Kashima Space Technology Center of NICT, National Institute of Information and Communications Technology), which aims at obtaining better accuracy on geodetic solutions on the Joint US-Japan VLBI program (see Fig.1). With the WVR data, however, they could not get remarkable improvements on the geodetic solution. Since then no trial on the WVR developments has been made in Japan except for a trial test of a water vapor spectrometer attached on a 10-m radio antenna located at the Usuda Deep Space Center. The work is performed by Yoshiharu Asaki in 2005 but not applied to actual VLBI observations. In 2015, the KEK, High Energy Accelerator Research Organization in Japan has succeeded to measure the wideband spectrum of a resonance pattern caused by a water vapor molecule in the atmosphere as shown in Fig.2.

The success inspires developments of a new advanced WVR in Japan. In the next section the current state of the WVR developed and operated in the world is overviewed. In Section 3, a serious problem on the WVR happened at a bad weather condition of a thick cloud and heavy raining is discussed. In section 4, a new WVR design on a wide band spectrometer with a high speed AD converter is proposed.

2. WVRs in the world

The Onsala Space Observatory has been working on the WVR (Forkman 2003)[1] which is shown in Fig.3. At a time when the receiver is in the calibration cycle, the mirror switches the beam to sky and a hot load behind the mirror alternatively. This calibration method is now widely employed to current WVRs for calibrating power measurements to sky noise temperature.

The JPL developed a new advanced WVR to correct the wet path delay for deep space navigation (Tanner 2003)[2]. It is a highly stable radiometer designed carefully to keep environment temperature in the receiver box within 0.004 degree (see Fig.4). The temperature stability is a key to get high stability in sky noise measurements[3](4)[5]. In

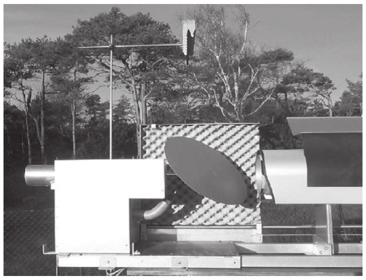

Figure 3. The Onsala WVR[1]

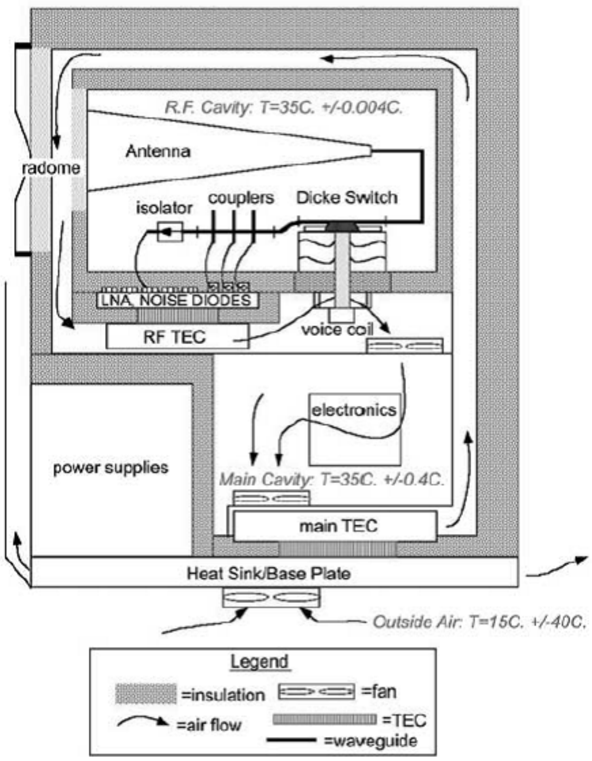

Figure 4. A hgihly temperature stabilized receiver of the JPL AWVR

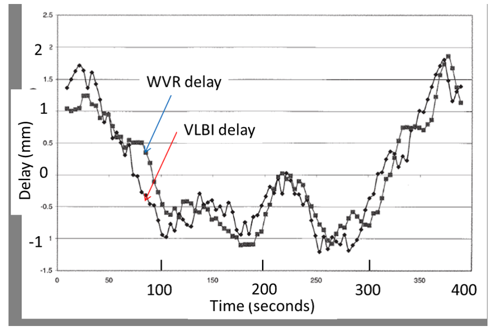

Figure 5. The mm accuracy of WVR excess path demonstrated with VLBI [6]

the sky noise measurement, noise temperature and gain of a receiver shall be kept constant together with physical temperature of the hot load, otherwise the sky noise originated in the water vapor emission in the sky is measured wrong.

Tahmoush & Rogers (2000)[6] shows good agreement on the wet delay less than 1 millimeter between the WVR delay and the VLBI delay as shown in Fig. 5.

Shanghai Astronomical Observatory operates a WVR at the Sheshan site nearby the Tianma 65m. The similar radiometers are prepared for all four VLBI stations in Chinese VLBI Network (CVN), Shanghai, Beijing, Urumuqi and Kunmin. Fig. 6 show the WVR located at the Tianma 65msite, which was first introduced in 2013 and expected to work with a high frequency VLBI at 22 and 43 GHz to be done with the 65m telescope. The WVR is expected to use in the correction of the atmospheric phase fluctuation in order to get a long coherence time and to make the sky absorption correction as well.

Figure 6. The WVR at the Tianma 65-m site of Shanghai Astronomical Observatory, China

The WVR receives sky noise emission in dual frequency channels, 23.8 and 31.4 GHz, each bandwidth of which is 500MHz. It has an absorber for the hot load calibration at the bottom of the receiver cabin. From the sky noise measurements on the dual frequency channels, it produces the EPL, Excess Path Length, in the unit of millimeter. The result will be shown in the next section.

IRAM WVRs have three receiving channels as shown in Fig. 7 and were used to correct interferometer phase as shown in Fig. 8 (Bermer(2010)[7]).

The university of Bern developed a WVR shown in Fig. 9 (Bleisch(2011)[8]. The WVR has an unique calibration system of a hot bar which partially cover the beam toward the sky.

A sensitive narrow band spectrometer succeeded to detect water vapor in the stratosphere (Kämpfer(2003))[9]. The spectral is so sharp in the feature due to the extremely low pressure that the high resolution spectrometer is a key of the detection together with high sensitivity. The detection of the sharp spectrum clearly show the existence of water vapor in the stratosphere higher than 10km

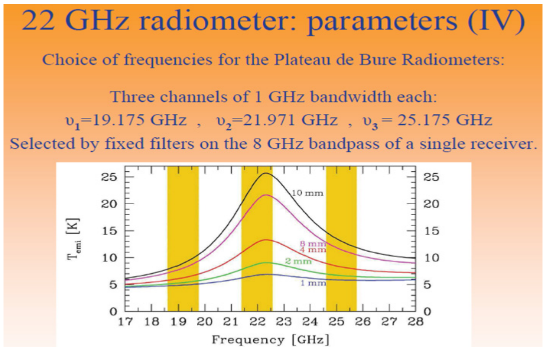

Figure 7. Three-channel radiometer developed by IRAM

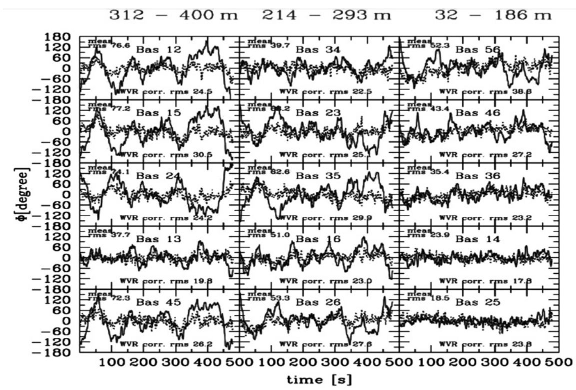

Figure 8. Interferometer phase corrected by WVR

above ground.

A WVR is working in Korea for the studies of middle atmosphere (DeWachter(2011))[10] in Sookmyung Women's University. The WVR is the same design as that of University of Bern.

3. Bad responses under cloud and rain

In Fig.12 the excess path lengths measured by SHAO WVR in comparison with GPS zenith delay and that derived with the Ray Trace method are shown on the day of May 31, 2016. At the CST time around 8h, the thick cloud covered the sky and at around 18h a heavy raining started. Under these

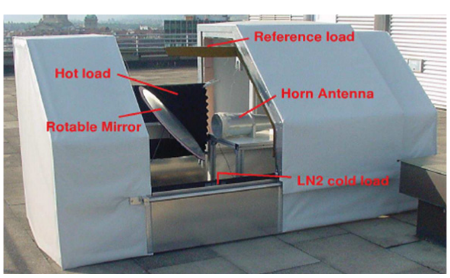

Figure 9. WVR developed by University of Bern, Switzerland

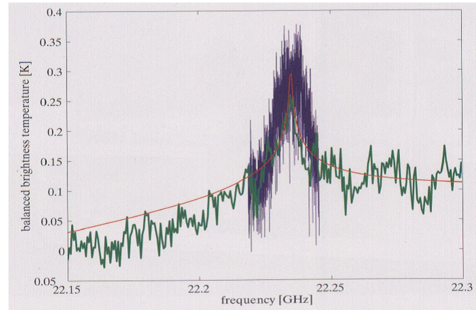

Figure 10. Water vapor in stratosphere, no pressure broadening spectrum[9]

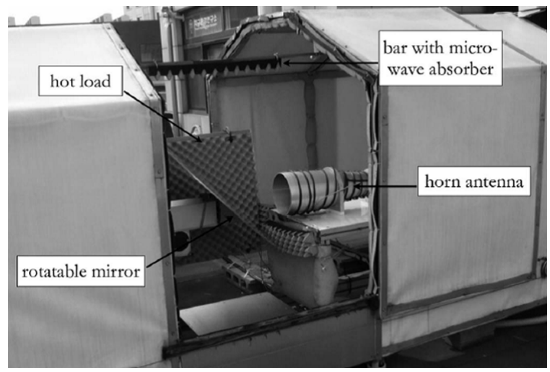

Figure 11. The WVR working in the Sookmyung Woman's University in Korea

bad weather conditions the EPL by SHAO WVR shows big errors compared to EPLs measured by GPS and Ray Trace. The incredibly large EPL of the WVR may come from the wrong conversion of the sky noise temperature onto the EPL. The sky noise increased with absorption by liquid water in a cloud and a rain is converted to the large EPL by an error. The imperfect separation of the EPL from the absorption may cause the large error.

The similar bad result was reported by Jung-ho Cho(2006)[11] as shown in Fig. 13. They compared the WVR EPL to the VLBI delay and found good agreement between them at the start of the day

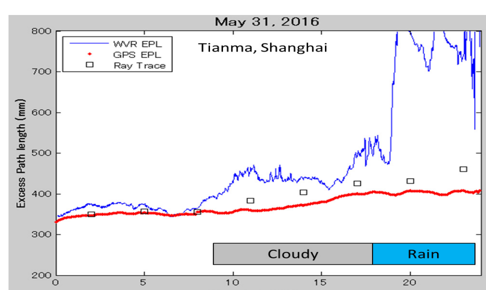

Figure 12. Excess path length measured by SHAO WVR in comparison with GPS and Ray Trace

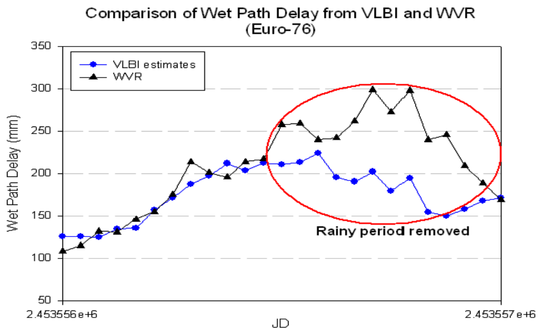

Figure 13. Measurement error of WVR under raining[11]

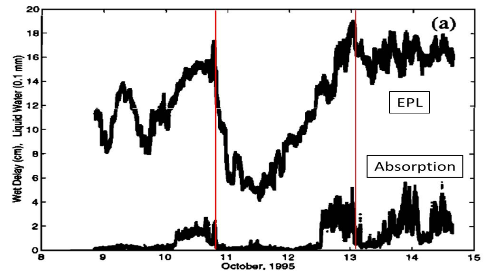

Figure 14. Separation of the excess path from absorption due to liquid water[12]

until the mid day but big discrepancy in the latter half of the day. They noted the discrepancy was caused by a rain.

Not only a rain but also a heavy cloud causes the big error in the WVR measurement owing to the imperfect separation of the vapor emission from the liquid water absorption. Both of the water vapor and the liquid water cause the rise in the sky noise temperature. We need to note that the liquid water absorption is almost constant or slightly linearly proportional to frequencies around the water vapor resonance peak at 22.2 GHz. We need to separate the water vapor emission by the resonance spectral pattern.

The perfect separation between absorption and delay was reported by Elgerd(1998)[12] with the Onsala WVR as shown in Fig. 14. The upper plot indicates the delay (EPL) and the lower absorption. The wet delay measured by the WVR is not affected by large absorption by the rain. Also we can see the rapid decrease in the wet delay after the rain stop. This is meteorologically understandable that a water vapor in the atmosphere is converted to the liquid water and fall down to a ground which causes the decreases in the water vapor content in the atmosphere. Even under raining, the WVR shows a reasonable value in the wet delay. This indicates that the careful analysis on the water vapor emission profile (resonance pattern around 22.2 GHz) makes possible to separate the wet delay from the liquid water absorption.

4. Technical points for future developments

By reviewing the current status of world WVRs and by considering the bad effect by cloud and rain, some technical points are described here.

4.1 Radiometer calibration

A radiometer measures the power in dimension of Watt and converts it to the brightness temperature of the sky in Kelvin by an equation, $P = kGB(T_{sky} + T_{rx})$, where P is a received power, k is the Boltzmann constant, G is a receiver gain, B is a receiver bandwidth, T_{sky} is a sky noise temperature and T_{rx} is a receiver noise temperature. If the receiver Gain, G, the bandwidth, B and the receiver noise temperature T_{rx} is stable and known, it is straight forward to convert the power to the sky noise temperature. The gain and the receiver noise temperature are, however susceptible to ambient temperature. This is a reason why we need to carefully keep the temperature of a receiver box. If we have two reliable references in the brightness temperature, T_{ref1} and T_{ref2}, and by putting these reference temperatures in place of T_{sky} we can solve for values of kGB and T_{rx}. Usually we use a hot load and a cold load for two reference brightness temperatures. The hot load is an absorber in a room temperature (~300K) and the cold load is an absorber dipped into a liquid nitrogen (~80K).

Another way is so called a Y-factor method, in which the power ratio is measured. The power ratio Y, $Y = \frac{P_{sky}}{P_{hot}}$, where P_{sky} is the power received by the WVR toward the sky and P_{hot} is the power terminated by the hot load. By taking the ratio, a common factor of kGB is canceled and we get the power ratio of Y as $Y = \frac{T_{hot}+T_{rx}}{T_{sky}+T_{rx}}$, and from the power ratio the T_{sky} is easily reduced by taking T_{hot} known. In advance to this Y-factor measurement, the receiver noise shall be measured by a hot/cold calibration, $Y' = \frac{T_{hot}+T_{rx}}{T_{cold}+T_{rx}}$ where T_{hot} and T_{cold} are known. Also it is assumed the T_{rx} is constant during sky noise measurements. A technical point on this method is a time how long we can keep the receiver noise temperature constant. Again it is important to keep the ambient temperature in the receiver box.

4.2 Spectrum measurement with a high speed AD

The SHAO WVR measures only two frequency channels and has not enough capability to separate water vapor from liquid water as mentioned in

Section 3. This is one reason why the WVR sometimes shows outrageous values in the excess path length. The best way to achieve ideal separation is to make measurement the frequency spectrum around the water vapor resonance as shown in Fig. 2. The resonance spectrum is fit to the theoretical one's and then the total amount of water vapor in the air is estimated. From the water vapor content in the air we can separately deduce the wet delay and the absorption.

The water vapor spectrum is widely spreading in frequency over a few GHz around the resonance peak frequency at 22.2GHz due to the high pressure in the lower atmosphere. Tahmoush(2000)[6] got the wide band spectrum by sweeping the frequency of a local oscillator in the frequency down converter. The Fig.2 measured by the KEK WVR is figured the spectrum by an analog spectrum analyzer. In both of them it takes a few seconds to a few tens seconds to get a full frequency span of the water vapor resonance. To correct a short term variation of the wet path, it is preferred to use a high speed AD converter and a digital spectrometer. The new digital water vapor spectrometer is now under development in Japan with a sampling frequency of 16GHz on the frequency band spanned from 16 to 24GHz. The author hope it will effectively work in the wet path correction in delay and absorption, and is used for precise astrometry and geodesy, and reliable imaging in radio astronomy.

5. Acknowledgments

The author would like to thank to Dr. M. Sekido for his great efforts in organizing this workshop and publication and is grateful to Dr. Bo Zhang, Ms. Yongchen Jiang and Mr. Shibiao Dou for their great support on my studies on the SHAO WVR. The author also expresses great thanks to Dr. Zhiqiang Shen and Dr. Qinghui Liu who give me a chance to study on a water vapor radiometer in Shanghai Astronomical Observatory.

References

[1] Peter Forkman, Patrick Eriksson, Anders Winnberg, The 22 GHz radio-aeronomy receiver at Onsala Space Observatory, Journal of Quantitative Spectroscopy & Radiative Transfer, 77, pp. 23-42, 2003

[2] Alan B. Tanner and A. Lance Riley, Design and performance of a high-stability water vapor radiometer, RADIO SCIENCE, VOL. 38, NO. 3, 8050, doi:10.1029/2002RS002673, 2003

[3] Balthasar T. Indermuehle,Michael G. Burton and Jonathan Crofts, Water Vapour Radiometers for the Australia Telescope Compact Array, Publications of the Astronomical Society of Australia, arXiv:1212.60101v2, 30 April 2013

[4] C. Straub, A. Murk, and N. Kämpfer, MIAWARA-C, a new ground based water vapor radiometer for measurement campaigns, Atmos. Meas. Tech., 3, 1271–1285, 2010

[5] Michael Britcliffe, Daniel Hoppe, and Manuel Franco, A Low-Cost Water Vapor Radiometer for Deep Space Network Media Calibration, IPN Progress Report 42-188, February 15, 2012

[6] David A. Tahmoush and Alan E. E. Rogers, Correcting atmospheric path variations in millimeter wavelength very long baseline interferometry using a scanning water vapor spectrometer, Radio Science, Volume 35, Number 5, Pages 1241–1251, September-October 2000

[7] Michael Bremer, Atmospheric Phase Correction, 7th IRAM Millimeter Interferometry School, Grenoble, October 4-8, 2010

[8] R. Bleisch, N. Kämpfer and A. Haefele, Retrieval of tropospheric water vapour by using spectra of a 22 GHz radiometer, Atmos. Meas. Tech., 4, 1891–1903, 2011

[9] Nikiaus Kämpfer, Beat Deuber, Dietrich Feist, Daniel Gerber, Christian MCtzler, Lorenz Martin, June Morland, Vladimir Vasic, Berne, Microwave Remote Sensing of Water Vapor in the Atmosphere, Geographica Helvetica Jg. 58 2003

[10] Evelyn De Wachter, Alexander Haefele, Niklaus Kämpfer, Soohyun Ka, Jung Eun Lee, and Jung Jin Oh, IEEE TRANSACTIONS ON GEOSCIENCE AND REMOTE SENSING, VOL. 49, NO. 3, pp. 1052-1062, MARCH 2011

[11] Jung-ho Cho, Axel Nothnagel, Alan Roy, and Ruediger Haas, A generalized scheme to retrieve wet path delays from water vapor radiometer measurements applied to European geodetic VLBI network, 4th IVS General Meeting, Concepcion, Chile, Jan. 9-11, 2006

[12] Gunnar Elgered and Per O. J. Jarlemark, Ground-based microwave radiometry and long-term observations of atmospheric water vapor, Radio Science, Volume 33, Number 3, Pages 707-717, May-June 1998

Status on the Ishioka Geodetic Observing Station

Masayoshi Ishimoto
(*ishimoto-m96pu@mlit.go.jp*),
Michiko Umei, Takahiro Wakasugi, Ryoji Kawabata, Tomoo Toyoda, Basara Miyahara, Yoshihiro Fukuzaki

Geospatial Information Authority of Japan, Kitasato-1, Tsukuba, Ibaraki, Japan

Abstract: The Geospatial Information Authority of Japan (GSI) has constructed a new VGOS station, which is named Ishioka Geodetic Observing Station. The construction of the antenna (radio telescope) was completed in March 2014, and an operation building was constructed in February 2016. At present we carry out legacy S/X-band international observations and temporarily install the equipment for broadband observations, including front-end and back-end.

We report the geodetic results of the legacy S/X-band observations and trial broadband observations carried out at Ishioka in collocation with five IVS stations.

1. Introduction

The Geospatial Information Authority of Japan (GSI) has constructed a new geodetic observing facility since 2011. This facility is designed for the next-generation VLBI system called VGOS, which is promoted by the International VLBI Service for Geodesy and Astrometry (IVS). The construction of the VGOS antenna was completed, and the other necessary equipment (front-end, back-end, hydrogen masers, and so on) was also delivered in March 2014. The detailed specifications of the antenna and the delivered equipment are reported in Fukuzaki et al. (2015). Construction of an operation building was then completed in February 2016. This new geodetic observing facility, called Ishioka Geodetic Observing Station, will be a main geodetic VLBI station in Japan as the successor of the Tsukuba 32-m station from 2017.

At present we carry out the legacy S/X-band international observations at both Ishioka and Tsukuba in order to obtain a precise tie vector between these two antennas. Ishioka started the legacy S/X-band observation in 2015, and continued the observation until July 2016. Ishioka will resume the legacy S/X-band observation in October 2016 after an interruption of two months during which we carry out trial broadband observations at Ishioka.

In August and September 2016, we set up the broadband observing system and carried out the broadband observations at Ishioka. Two kinds of broadband feeds were available at Ishioka: One is the Eleven feed developed by the Chalmers University of Technology in Sweden, and the other is the Quadruple-Ridged Flared Horn (QRFH) developed by California Institute of Technology. We evaluated receiving performance of these feeds. We also developed the frequency Up-Down Converter and the K6/iDAS Sampler for the broadband system and evaluated their operational performance. Then Ishioka carried out the broadband observations using these equipment.

This paper gives the results of the legacy S/X-band observations and the present status of the equipment and the broadband observations.

2. Observing facility

The Ishioka Geodetic Observing Station is located at about 17 km northeast of the Tsukuba station. Figure 1 shows the location and an overview of the Ishioka station. Since the Ishioka station is designed to contribute to Global Geodetic Observing System (GGOS) as a core observatory, it has a GNSS CORS (Continuously Operating Reference Station) and a gravity measurement facility in addition to the VGOS antenna.

Figure 1. Location and overview of Ishioka Geodetic Observing Station

3. Result of the legacy S/X-band observation

The Ishioka station carried out the first legacy S/X-band observation in January 2015, and forty-six 24-hour observations were carried out in total until July 2016. Table 1 shows the number of observations carried out at Ishioka. Figure 2 shows time series variation of the estimated baseline length between Ishioka and the Tsukuba 32-m antenna. There are two interruptions during the observations because of re-adjustment of the equipment and construction of the operation building. The average of standard deviations of the five observations before September 2015 is about 3 mm and quite large, because artificial radio signals in the frequency range less than 2.1 GHz were strong enough to degrade observation signal quality in the range. Therefore we installed a high pass filter to cut less than 2.2 GHz, a notch filter to cut 2.1 GHz, and a band pass filter to pass 2.2-2.4 GHz after the Low Noise Amplifier output. As a result, the average of standard deviations after September 2015 is significantly improved and about 1 mm.

Table 1. Number of observations

Session Type	Number of observations
JADE	17
AOV	9
IVS-R1	17
IVS-T2 etc	3
Total	46

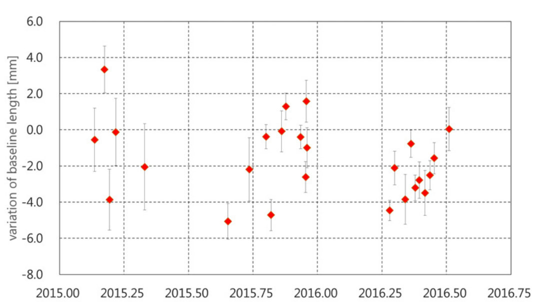

Figure 2. Variation of baseline length between Ishioka and Tsukuba 32m antenna

4. Status of equipment for broadband observation

4.1 Front-end

Eleven feed and QRFH were evaluated as candidates for a broadband feed at Ishioka. We found that SEFD (System Equivalent Flux Density) values of Eleven feed were higher than that we expected for over 10 GHz frequency (e.g., 7500 Jy for 14 GHz) (Fukuzaki et al, 2015). Then, we measured SEFD values of QRFH to evaluate the receiving performance. The SEFD values of QRFH are shown in Figure 3. These values were measured using the radio signals from a strong radio source, Taurus-A. This figure shows that the SEFD values of QRFH are reasonably good from 3 GHz to 14 GHz. The signals less than 3 GHz were cut by a high pass filter, because the radio signals from Radio Frequency Interference sources were strong enough to cause saturation of the receivers. In conclusion, we determined to employ the QRFH system as the broadband feed.

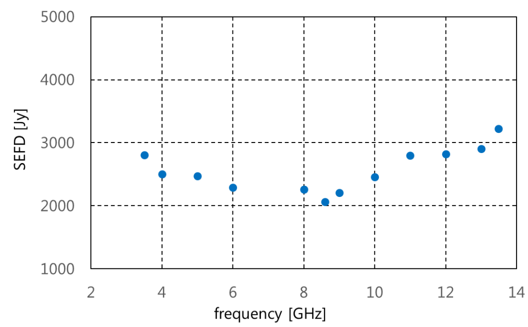

Figure 3. SEFD values of Ishioka VGOS antenna with QRFH

4.2 Frequency Up-Down Converter

We developed a new frequency converter, the frequency Up-Down Converter, compliant with the VGOS concept. This converter selects any 1 GHz bandwidth signal between 2 GHz and 14 GHz and converts the frequency to 1-2 GHz band. This equipment composes one control unit and four conversion units (Figure 4). One conversion unit has two outputs for both horizontal and vertical polarization components. Therefore four bands (eight channels) signals can be handled in total. In this equipment, input signal is first up-converted to 28 GHz band and then down-converted to 1-2 GHz band. The block diagram of this equipment is shown in Figure 5. Because the local oscillator frequency for up-conversion is programmable between 15.440 GHz and 26.416 GHz, any 1 GHz bandwidth signal between 2 GHz and 14 GHz can be converted to 1-2 GHz band.

4.3 Sampler

We developed a new sampler called K6/iDAS. The specifications of K6/iDAS are listed in Table 2. The K6/iDAS supports two sampling modes:

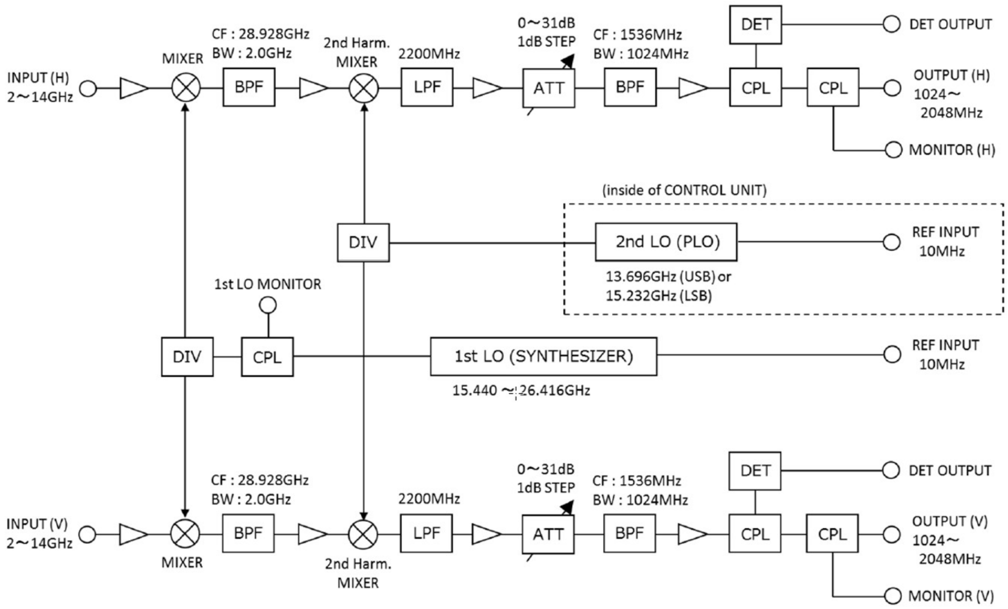

Figure 5. Block Diagram of frequency Up-Down Converter for one conversion unit

Figure 4. Photo of frequency Up-Down Converter installed at Ishioka station

Table 2. Specifications of K6/iDAS sampler installed at Ishioka station

Parameter	**Value**
wide-band mode	
maximun data rate	4096 Mbps
sampling rate	256, 512, 1024, 2048 Msps
bits	1-8 bit
channels	1
DBBC mode	
maximun data rate	4096 Mbps
sampling rate	8, 16, 32, 64, 128 Msps
bits	1-8 bit
channels	1, 2, 4, 8

One is wide band mode, which samples 1 GHz bandwidth directly with 4 Gbps (2 bit and 2 GHz) recording rate, the other is Digital Base Band Converter (DBBC) sampling mode. Since this sampler is under evaluation, we also use ADS3000+ AD Samplers developed by National Institute of Information and Communications Technology (NICT) and Institute of Space and Astronautical Science (ISAS) for broadband observations.

4.4 Broadband observation

Ishioka carried out the first international broadband observation with the Hobart 12-m antenna in Australia and the Kashima 34-m antenna in Japan on 9 August 2016. The details of this observation are shown in Table 3. The first fringes of the international broadband observation for Ishioka were detected between Ishioka and Hobart. In the case of this observation, our frequency Up-Down Converter and K6/iDAS Sampler were not used, instead, another AD sampler K6/GALAS, which was developed by NICT (Sekido et al., 2015), was used.

After the observation Ishioka participated in the other two broadband observations (VGT003 and VGT004) planned by IVS on 11 and 30 August (Table 3). The fringes were not detected for VGT003 probably due to incorrect frequency settings. On the other hand, for VGT004, the fringes were detected successfully. This is the first fringe for our

Table 3. details of Broadband observations

Parameter	**Value**
HK16222 with Hobart and Kashima	
Date	9 and 10 August 2016
Frequency (center)	4360, 5112, 9960, 12860 MHz
Bandwidth of one band	1024 MHz
Sampling rate	2048 Msps
bits	2
Polarization	Vertical
channels	1 ch x 4 bands
VGT003 and VGT004	
Date	10 and 30 August 2016
Frequency (center)	3240.4, 5480.4, 6600.4, 10440.4 MHz
Bandwidth of one band	512 MHz
sampling rate	1024 Msps
bits	2
Polarization	Horizontal and Vertical
channels	16 ch x 4 bands

new system with frequency Up-Down Converter and ADS3000+ AD Sampler. For the next step Ishioka will carry out an international 24-hour broadband observation in September 2016.

5. Summary

Construction of the Ishioka Geodetic Observing Station was completed in February 2016. Ishioka has mainly carried out the legacy S/X-band observations, and the reasonable geodetic results were obtained. In addition, we almost finished installation of the equipment for the broadband observation at Ishioka. Ishioka carried out two international broadband observations in August 2016, and the fringes were successfully detected. Ishioka will carry out an international 24-hour broadband observation in September 2016 and resume the legacy S/X-band observations from October. In 2017, we will carry out both the broadband and the legacy observations.

6. Acknowledgments

We would like to thank colleagues of NICT Space-Time Measurement Group for their generous assistance on the broadband observations. We also acknowledge colleagues of NASA/GSFC and University of Tasmania for their cooperation in the broadband observations.

References

[1] Fukuzaki, Y., K. Wada, R. Kawabata, M. Ishimoto, and T. Wakasugi, First Geodetic Result of Ishioka VGOS Antenna, IVS NICT-TDC News No.35,pp.1-3,2015.

[2] Sekido, M., K. Takefuji, M Tsutsumi, and T. Kondo, Broadband VLBI Data Acquisition System for GALA-V, IVS NICT-TDC News No.35,pp.7-11,2015.

Development of Wideband Antenna

Hideki Ujihara (*ujihara@nict.go.jp*)
*Kashima Space Technology Center,
National Institute of Information
and Communications Technology,
893-1 Hirai, Kashima, Ibaraki 314-8501, Japan*

1. Status of development

New wideband feed, NINJA Feed, has installed in the Kashima 34m antenna in the last summer. The NINJA feed was designed for 3.2-14.4 GHz and was mounted nearby the IGUANA Daughter feed which is operated in 6.5-15 GHz band as shown in Figure 2. The main reflector of the MARBLE at NICT Koganei was enlarged from 1.6 m to 2.4 m and its optics was changed to the Cassegrain with another type of the NINJA, as shown in Figure 3. They are operated with 30-40 % aperture efficiency, but receiving frequencies of both antennas are limited by the WRD350 to SMA converters now. Also new wideband OMT for these NINJA feeds was developed as shown in Figure 1. This OMT was tested with the NINJA feed in the 34 m antenna, but strong RFI from cellular phones in 2 GHz band was received. Thus observations with dual polarization will not be started after new OMT is designed and fabricated.

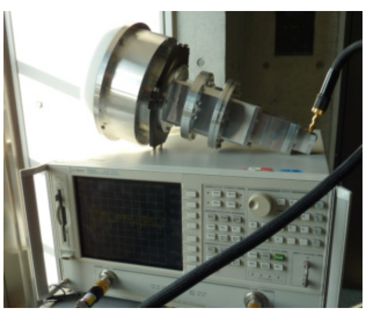

*Figure 1.
Return loss measurement of the new wideband OMT with the NINJA feed for the MARBLE.*

2. Plans

New wideband OMT and NINJA feeds will be developed in this year to replaced the current NIJNA feeds. They can cut RFI in the 2 GHz band and will improve the aperture efficiencies of our 34 m and 2.4 m antennas. Observations with dual polarization will be started soon after the replacement of the NINJA feed in the 34 m. Wideband OMTs will be developed for the IGUANA feeds.

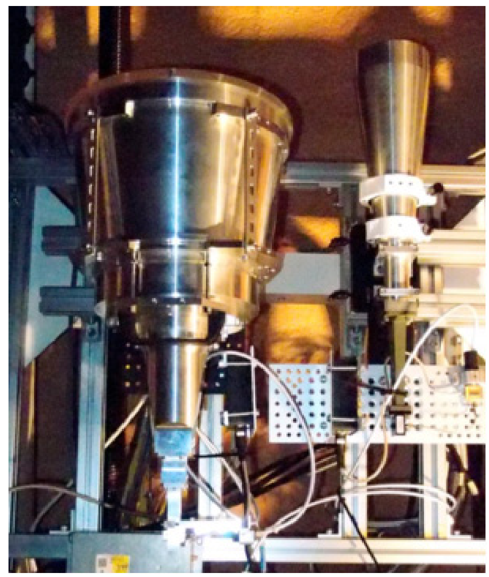

*Figure 2.
The NINJA feed and the IGUANA feed in the Kashima 34m receiver cabin.*

*Figure 3.
MARBLE 2.4m on the roof top of the NICT KOGNEI 2nd building.*

Development Status of GALA-V Broadband VLBI — Geodetic Solution and Clock Comparison –

M. Sekido[1] (*sekido@nict.go.jp*),
K. Takefuji[1], **H. Ujihara**[1], **T. Kondo**[1],
Y. Miyauchi[1], **M. Tsutsumi**[1], **E. Kawai**[1],
S. Hasegawa[1], **J. Komuro**[2], **R. Ichikawa**[2],
Y. Koyama[2], **Y. Hanado**[2], **K. Terada**[2],
K. Namba[2], **R. Takahashi**[2], **T. Aoki**[2],
T. Ikeda[2], **R. Kawabata**[3], **M. Ishimoto**[3],
T. Wakasugi[3], **Y. Umei**[3], **T. Toyoda**[3],
K. Watabe[4], **T. Suzuyama**[4] *1)*

NICT/Kashima Space Technology Center, 893-1 Hirai, Kashima Ibaraki, Japan.
2) NICT/Headquarter, 4-2-1 Nukui-Kita, Koganei, Tokyo 184-8795, Japan.
3) Geospatial Information Authority of Japan., 1, Kitasato, Tsukuba 305-0811, Japan.
4)National Meteorology Institute of Japan, Umezono, Tsukuba 305-8563, Japan

Abstract: Development of broadband VLBI system named GALA-V has been conducted by NICT for VLBI application to distant frequency transfer. Observation systems and signal chain from data acquisition to analysis has become ready. A series of broadband VLBI sessions with pair of small diameter antennas and high sensitivity antenna (Kashima 34m or Ishioka 13m) have been performed since Jan. 2016. VLBI delay data on the baseline between small antenna pair were not directly derived by the cross correlation of these data set, but that was computed by linear combination of delay observables between small antennas and high sensitivity antenna baselines. Geodetic solutions of seventy km baseline between 1.6m and 2.4m diameter antennas were obtained by the virtual observables. The repeatability of the station coordinates were several millimeters in horizontal and a few centimeter in vertical position. Atomic clock behaviors between two small stations are obtained from these VLBI sessions and they are consistent with those derived by GPS observations. This paper reports overview of the system development and data analysis results of broadband VLBI sessions in 2016.

1. Introduction

NICT is conducting development of broadband VLBI system named GALA-V for distant frequency transfer [1]. Broad observation frequency range 3-14 GHz has been motivated for improvement in sensitivity and delay measurement precision, and joint observations with VGOS stations are in the scope. The GALA-V system has target of making distant frequency comparison between transportable small VLBI stations by the help of joint observation with high sensitivity VLBI stations. Advantages of using small antennas are mainly two folds. Firstly, features of lower cost and transportability are suitable as a tool for frequency comparison of atomic time standards. Secondary, large diameter antenna has potential cause of delay fluctuation such as distortion of antenna structure and long signal transmission lines. Those effects related with large diameter antenna are canceled out in the linear combination of the equation (1). Magnitude of distortion is proportional to the size of the antenna, thus potential error sources are reduced for small antenna.

Signal to noise ratio (SNR) of VLBI observation is proportional to the products of two observing stations of the baseline. Thus disadvantage of lower sensitivity of small antenna pair (A and B) is compensated by joint observation with high sensitivity station (R). Even SNR was not enough on A-B baseline, as far as R-A and R-B baselines works as interferometer, delay observable of small antenna pair τ_{AB} can be computed by linear combination

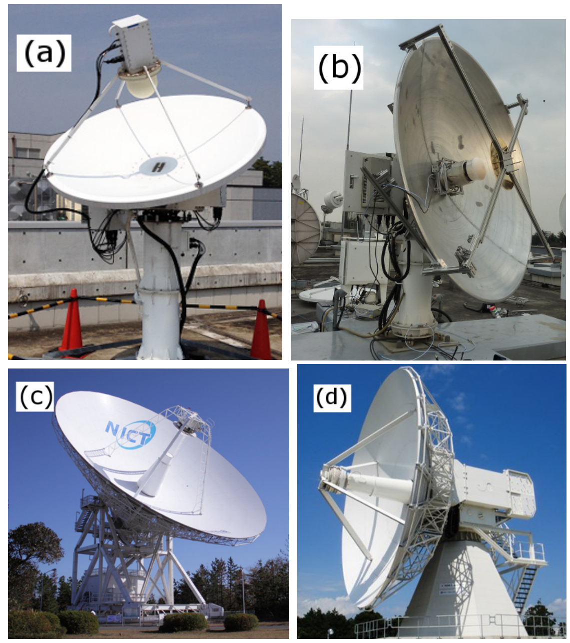

Figure 1. Pictures of VLBI antennas, which are capable of broadband observation in Japan. (a) MARBLE1 1.6m, (b)MARBLE2 2.4m, (c) Kashima 34m, (d) Ishioka 13m.

of delay observable $\tau_{\rm RA}$, $\tau_{\rm RB}$ as follows:

$$\begin{aligned}\tau_{\rm AB}(t_{\rm prt}) = \\ \tau_{\rm RB}(t_{\rm prt} - \tau_{\rm RA}(t_{\rm prt})) - \tau_{\rm RA}(t_{\rm prt} - \tau_{\rm RA}(t_{\rm prt})) \\ \cong \tau_{\rm RB}(t_{\rm prt}) - \tau_{\rm RA}(t_{\rm prt}) - \\ \frac{d}{dt}\tau_{\rm AB}(t_{\rm prt}) \times \tau_{\rm RA}(t_{\rm prt}) \quad (1)\end{aligned}$$

It should be noted that this is valid when the radio source is supposed as a point source with respect to the fringe spacing in the sky formed by the projected baseline. Radio source structure effect have to be considered when the brightness distribution of the radio source is not negligible. This assumption is valid for the experiments described in this paper due to short baselines.

Based on this idea, broadband VLBI stations of small antenna pair and high speed data acquisition systems have been developed. Fig. 1 shows VLBI stations, which is capable of broadband observation in Japan. Kashima 34m station and small diameter broadband stations MARBLE1 and MARBLE2 have become ready for operational broadband observations in 2016. Ishioka 13m station of Geospatial Information Authority of Japan (GSI) has started its operation since 2015. This report describes current status of broadband system development, and some results of broadband VLBI sessions conducted in 2016.

2. Development of Broadband VLBI System GALA-V

2.1 Broadband VLBI Antennas

Kashima 34 m diameter VLBI station has been upgraded by installation of our original broadband feed systems. The first prototype feed IGUANA-H, which has sensitivity at 6.5-15 GHz[2, 3], was installed in 2014. The next feed NINJA was designed for 3.2-14.4 GHz frequency range[4], and it was mounted on the 34 m antenna in 2015. System temperature and System Equivalent Flux Density (SEFD) are about 200-300 Kelvin and 1500-2000 Jansky for 3-11 GHz frequency range, respectively[5].

A pair of small diameter antennas MARBLE1 and MARBLE2 have been originally developed for the project of baseline evaluation[6]. Both of these antennas are equipped with Rindgren Quadridge Flared Horn (QRFH)s and room temperature LNAs, and frequency downconverter for S/X-band had been used in that project. We have upgraded them to enable broadband observation for GALA-V project. One of two broadband transportable antennas (MARBLE1 of 1.6m diameter) has been installed at National Institute of Metrology in Japan (NMIJ) at Tsukuba. The other antenna (MARBLE2 of 1.5m diameter) has been placed at NICT headquarter at Koganei.

MARBLE2 1.5 m diameter prime focus antenna using QRFH was upgraded to 2.4 m dish of Cassegrain optics with second NINJA feed in 2016. By using room temperature LNA, the system noise temperature is around 150-200 Kelvins in 3-11 GHz frequency range. After that evaluation of second NINJA feed at MARBLE2, the third NINJA feed will be installed to MARBLE1 antenna, and diameter of the antenna will be upgraded to 2.4 m with Cassegrain optics in near future. Current system noise temperature of MARBLE1 antenna is 200-300 Kelvins.

Both of two small antennas are capable of only single linear (Vertical) polarization observation. Current SEFDs of MARBLE1 and MARBLE2 are $1 \sim 2 \times 10^6$ Jansky, and $2 \sim 4 \times 10^5$ Jansky, respectively in 3-11 GHz frequency range.

2.2 Data Acquisition and Signal Processing

Another new technology introduced in this project is "RF-Direct-Sampling" technique[7], which converts radio frequency analog signal to digital data by using high speed sampler K6/GALAS[8] at 16,384 MHz sampling rate without analog frequency conversion. Four bands of signals with 1 GHz bandwidth can be flexibly specified in 0 - 16 GHz frequency range, and they are extracted by digital signal processing. Then the data is acquired to high speed recording system through 10G-Ethernet interface. This RF-Direct-Sampling technique has an essential advantage at stable phase relation between the signals of each bands. Since precise group delay observable is obtained by linear phase gradient over broad frequency range, phase distortion caused by the signal transmission line from the radio telescope to the recording system has to be calibrated. Linear phase characteristics is the key feature to measure precision group delay with broadband signal. In case of analog frequency conversion, it is inevitable that unpredictable phase offset originated from local oscillator is added in that process. Conventionally, phase calibration signal (Pcal)[9] has been used to calibrate phase characteristics of the system including the offset and signal transmission path, however special care is needed to keep phase stability of the Pcal device itself. Because the timing of Pcal signal is triggered by reference signal, thus its phase can be changed by thermal extension of reference signal transmission cable. For monitoring and calibration of this change, Delay calibration system (Dcal) has been used at geodetic VLBI

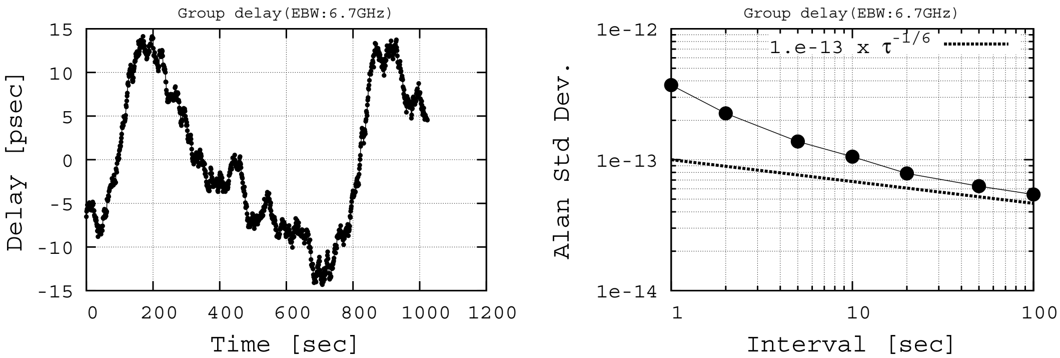

Figure 2. Left panel shows time series of broadband VLBI delay data for 3C273B on Kashima 34m - Ishioka 13m baseline. Trend of slow delay change including geometry and clock has been subtracted by polynomial fitting. Every points of 1 sec. interval represents delay data obtained by synthesizing four frequency bands. The random walk like delay behavior, which changes about 20 ps in a few hundred seconds, might be caused by atmospheric delay fluctuation. Right panel shows Alan standard deviation computed from the delay data in the left panel. Dashed line indicates $\sigma(\tau) = 1 \times 10^{-13}\tau^{-1/6}$*, which is an example of fluctuation evaluated by Kolmogorov turbulence theory and coefficient in literatures[12, 13].*

stations. Whereas in case of RF-Direct-Sampling, phase relation among the four bands of signal is frozen at the point of digitization.

For recovery of linear phase characteristics over the wide frequency range, we employed a phase calibration method using reference radio source. Radio sources with relatively stronger flux are observed a few times in a session, then one of the scans with high SNR is chosen as template for calibration. The cross correlation phase spectrum of the template scan data is applied to all the scans of whole session to calibrate the phase characteristics of signal transmission path and data acquisition. This method has been proven to work well in our broadband VLBI sessions.

Polarization of the data acquisition in our VLBI sessions has been only single linear (Vertical) polarization. Because differences of paratactic angles are negligible on these domestic short baselines, this it not a issue at present. Dual polarization observation is necessary in intercontinental long baseline observation. And the VGOS specification requires dual linear polarization observation, Dual polarization data acquisition is being prepared in out GALA-V project, too.

Cross correlation of the data has been processed by using high speed software correlator GICO3 [10], which was developed by NICT for astronomical broad band observation. Correlation output of four band of signals are synthesized by new wideband bandwidth synthesis (BWS) software 'komb'[11]. The BWS produces sharp peak in time domain after phase characteristic calibration by using template scan as described above. Fig. 2 shows a delay data of radio source 3C273B obtained by a test experiment on Kashima 34m - Ishioka 13m baseline in 2015. The data shows that sub-pico second delay precision was achieved by 1 second of observation. It is demonstrating potential of extremely high delay precision by the broadband observation system. The random walk like that delay behavior, which changes about 20 ps in a few hundred seconds, is thought to be caused by property atmospheric delay change. Alan standard deviation of the data shows consistent trend with an example of fluctuation (dashed line in the right panel of Fig.2) evaluated by Kolmogorov turbulence theory and coefficient in literatures [12, 13].

3. Broadband VLBI Sessions in 2016

Basic observation mode of the GALA-V system was allocating four 1024 MHz width data acquisition bands in 3-14 GHz frequency range with non-redundancy interval. Frequency allocation of band center at 4.0 GHz, 5.6 GHz, 10.4 GHz, and 13.6 GHz was the original plan. Although by taking into account practical condition such as radio frequency interference (RFI) and sensitivity of current receivers, slightly narrow frequency allocation at 5.9, 7.1, 8.7, and 10.6 GHz was used in the VLBI sessions in 2016.

Eight broadband VLBI sessions have been conducted during period between January to September 2016 (Table 1). Because the target of the project is frequency comparison of atomic standards, then session lengths are longer than 24 hours to get clock behavior in long time span. Extracted observation data of broadband VLBI sessions are stored to MK3 database and analyzed by Calc Ver.11.01 and SOLVE Release 2014.2.21 de-

Table 1. Broadband VLBI sessions during Jan.-Sep. in 2016. Kas34:Kashima 34m antenna, MBL1: MARBLE1 antenna, MBL2: MARBLE2 antenna, Ish13: Ishioka 13m antenna.

Date in 2016	Stations	Num. Scans Used/Recorded	Session Duration	Avg. time /scan
26-27 Jan.	Kas34—MBL1—MBL2	1330/1500	46 h	110 sec.
12-13 Feb.	Kas34—MBL1—MBL2	1250/1600	47 h	106 sec.
28-29 Feb.	Kas34—MBL1—MBL2	1050/1450	49 h	122 sec.
16-17 May.	Kas34—MBL1—MBL2	1220/1410	31 h	79 sec.
24-25 Jun.	Kas34—MBL1—MBL2	1800/1850	49 h	95 sec.
10-11 Jul.	Kas34—MBL1—MBL2	1960/2003	48 h	86 sec.
23-24 Aug.	Ish13—MBL2	1372/1385	43 h	112 sec.
12-13 Sep.	Ish13—MBL1—MBL2	1600/1640	35 h	77 sec.

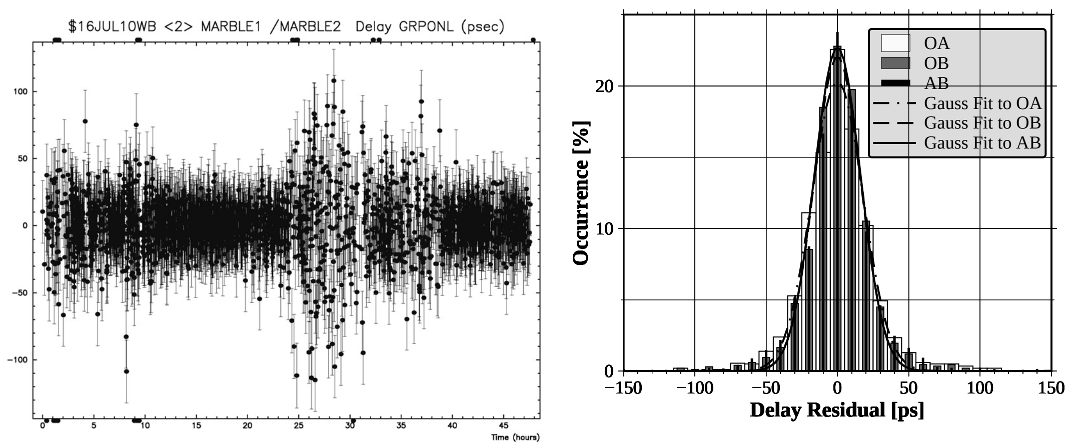

Figure 3. Post-fit delay residual of AB baseline in the session of 10-11 July, where delay of AB baseline was computed by linear combination of OA, and OB baselines. (O:Kashima34, A: MARBLE1, and B:MABLR2). Delay errors evaluated from SNR of BWS results was 4 ps or below for all the scans of AB baseline. Extra noise of 23 ps was added in the reweighting procedure to make reduced χ^2 unity.

veloped by NASA/GSFC(`http://gemini.gsfc.nasa.gov/solve/`). Estimation parameters in VLBI analysis are station coordinates (XYZ), atmospheric delay with Niell's Mapping Function with 20 min. interval, and clock parameters in 60 min. interval. Since there is no ambiguity in our delay observable due to broad bandwidth, analysis procedure is simply flagging bad data and reweighting of data to make reduced-χ^2 unity. Delay residual of small antenna pair AB baselines in the session of 10-11 July is displayed in Fig.3.

As described at introduction, correlation processing for AB baseline is not performed, but the delay data of AB baseline is computed by linear combination of delays of OA, OB baselines with equation (1). Delay error magnitude of AB baseline is supposed to increase as root sum square of the error of OA and OB baseline via error propagation law. However, post fit delay residual of AB baseline does not increase as expected. This indicates the post fit residual is dominated by extra error added to make reduced-χ^2 unity, which is added in the baseline analysis and that represents un-modeled delay error. This suggests that degradation of delay error by linear combination process was negligible in these broadband sessions. A series of MARBLE2 station coordinates estimated with AB baseline data of broadband sessions are displayed in Fig. 4. By taking into account a linear trend of -10.5 mm/yr in E-W direction, repeatability of horizontal coordinates was about several milli-meters, and that of vertical coordinates was a few centimeters. Estimated 'Clock+residual' as the product of VLBI is plotted in Fig. 5. Their clock behavior is consistent with GPS ppp-solutions, though variation around the trend is larger on VLBI. Further improvement need to be investigated.

4. Summary

Broadband VLBI system GALA-V acquiring four 1 GHz band width in 3-14 GHz frequency range has now been ready for single linear polarization observation. Original designed broadband

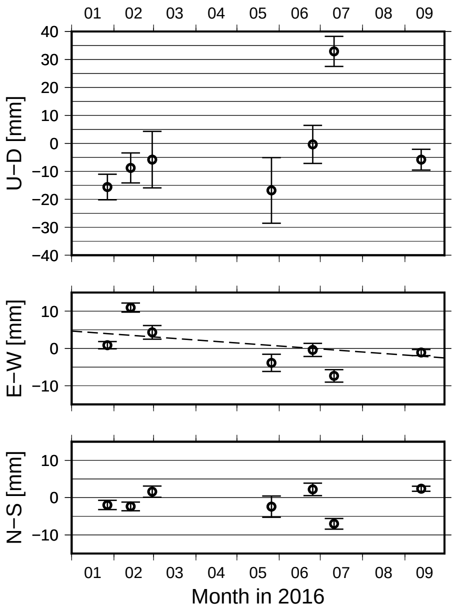

Figure 4. Series of MARBLE2 station coordinates estimated with AB baseline data are displayed for UP-Down, East-West, and North-South coordinates. Error bars of each point indicates formal error of the coordinates in each session. A linear trend of -10.5 mm/yr was observed in East-West direction, which we suppose to be due to local effect. By taking into account removing this trend only in East-West coordinates, repeatability of the MARBLE2 station coordinates w.r.t the MARBLE1 coordinates are several milli-meters in horizontal and about a few centi-meters in vertical coordinates.

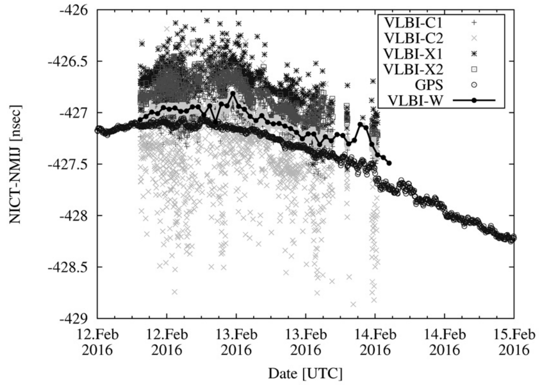

Figure 5. An example of 'Clock+residual' obtained by VLBI data in Feb. 12-14 session is plotted. Marks of ('+', 'x', '','□') are solution of single 1 GHz band at 5.9 GHz, 7.1 GHz, 8.7 GHz, and 10.6 GHz. The solid line and closed circle is broadband delay by synthesis of all bands. GPS analysis results is plotted with open circles. Vertical position of the VLBI data is shifted appropriately for comparison.*

feeds have been developed to satisfy the conditions of broadband receiving and narrow beam width for Cassegrain focus. A new technique RF-Direct-Sampling by using K6/GALAS sampler demonstrated simplified data acquisition system without Pcal device. This system is working effectively for stable broadband delay measurement. Broadband bandwidth synthesis software was developed and it resulted ever achieved sub-pico second group delay measurement by broadband VLBI experiment. A series of broadband domestic VLBI sessions with GALA-V system have been conducted. VLBI delay data on the baseline of small diameter antenna pair were computed by linear combination of delay data with respect to larger antenna, and it was analyzed by CALC/SOLVE system. Repeatability accuracy of the geodetic solution of small antenna pair was several millimeters and a few centimeters in horizontal and in vertical coordinates, respectively. Atomic clock difference estimated a by VLBI observation between small diameter antenna pair has been successfully estimated. It shows consistent results with that measured by GPS observation.

Dual linear polarization observation will be indispensable in intercontinental broadband VLBI observation. Source structure effect may have to be considered in long baselines. We need development of data processing scheme of mixed polarization data, and further improvement of precision is subject for the next step.

5. Acknowledgments

Development of broadband receiver system was supported by grant (2013 -2014) of Joint Development Research from National Astronomical Observatory of Japan(NAOJ). We appreciate the support from research network provider JGN for high speed network environment.

References

[1] M. Sekido, K. Takefuji, H. Ujihara, M. Tsutsumi, S. Hasegawa, Y. Miyauchi, E. Kawai, R. Ichikawa, Y. Koyama, and T. Kondo, "Status of Broadband VLBI Observation System (GALA-V) Development", IVS NICT-TDC News. No. 34, pp.17-19, 2014.

[2] H. Ujihara, K. Takefuji, M. Sekido, "Development of Wideband Feed" IVS NICT-TDC News. No. 34, pp.28-31, 2014.

[3] Ujihara, H., "Development of Wideband Feed for Kashima 34 m Antenna" submitted to Radio Science, 2016.

[4] H. Ujihara, K. Takefuji, M. Sekido, "Development of Wideband Feed" IVS NICT-TDC News. No. 35, pp.12-13, 2015.

[5] M. Sekido, et al., "An Overview of the Japanese GALA-V Wideband VLBI System", The 9th IVS General meeting Proceedings, in printing, 2016.

[6] R. Ichikawa, et al.., "MARBLE (Multiple Antenna Radio-interferometry for Baseline Length Evaluation): Development of a Compact VLBI System for Calibrating GNSS and Electronic Distance Measurement Devices", IVS 2012 General Meeting Proceedings "Launching the Next-Generation IVS Network" Edited by Dirk Behrend and Karen D. Baver, NASA/CP-2012-217504, pp.161-165, 2012.

[7] K. Takefuji, et al., "High-order Sampling Techniques of Aliased Signals for Very Long Baseline Interferometry", Publ. Astron.Soc. Pacific, Vol.124, pp.1105-1112, 2012.

[8] Mamoru Sekido, Kazuhiro Takefuji, Masanori Tsutsumi, and Tetsuro Kondo, "Broadband VLBI Data Acquisition System for GALA-V", IVS NICT-TDC News No.35., pp.7-11, 2015.

[9] T.Clark, et al., "Precision Geodesy Using the Mark-III Very-Long-Baseline Interferometer System", IEEE Trans. on Geosci. and Remote Sens., Vol., GE-23, No.4, 1985.

[10] M.Kimura, "Development of the software correlator for the VERA system III", IVS NICT-TDC News. No. 29 pp.12-14, 2008.

[11] Kondo, T., and K. Takefuji, "An algorithm of wideband bandwidth synthesis for geodetic VLBI", Radio Sci., 51, doi:10.1002/2016RS006070, 2016.

[12] Thompson.R, J. Moran, and G. Swenson, "Interferometry and Synthesis in Radio Astronomy", Krieger Pub. Com. 1994.

[13] Armstrong, J.W., and R.A.Shramek, "Observations of Tropospheric Phase Scintillations at 5GHz on Vartical Paths", Radio Sci., Vol 17, pp.1579-1586, 1982.

Performance of Direct Sampler K6/GALAS

Kazuhiro Takefuji (*takefuji@nict.go.jp*)

[1] *Kashima Space Technology Center, National Institute of Information and Communications Technology, 893-1 Hirai, Kashima, Ibaraki 314-8501, Japan*

Abstract:

We have been developing a broadband VLBI system so-called Gala-V, which meets the VGOS (VLBI2010 Global Observing System) requirements. The direct sampler, so-called K6/GALAS is a key component of the our project. Here we report an evaluation of K6/GALAS including jitter and frequency response.

1. The Direct Sampler, K6/GALAS

Figure 1 shows the design of K6/GALAS. It has four analog inputs and four 10 GbE outputs. K6/GALAS samples an input signal at 16 GHz speed and 3 bits quantization. K6/GALAS realized the down-conversion with high order sampling or digital baseband conversion of digital signal technique inside.

Actually, the RF signal of the range of 3 to 15 GHz from Kashima 34 meter radio telescope is transferred without frequency-conversion through high sensitivity optical fiber from antenna cabin to our observation room. Then, the signal after some amplified inputs to the K6/GALAS. Currently we installed the low-pass filter and high-pass filter of the frequency of 8 GHz before input the signal to the K6/GALAS because the frequency of 8.192 GHz is the half sampling speed (see Table 1).

2. Evaluation of K6/GALAS

2.1 Jitter measurement

The internal digital baseband conversion or high-order sampling method converts the high frequency signal to a baseband frequency. Thus, the direct sampler should have a high stability frequency response. This is expressed by "jitter" in time domain or "phase noise" in frequency domain.

At first, we evaluated the jitter performance. We input a sinusoidal signal from a signal synthesizer to K6/GALAS at each frequencies, then calculated the jitter from digitized signal. K6/GALAS samples the signal in 3 bit and 16.384 GHz sampling speed and the signal becomes down-converted digitally inside the sampler. We input several frequency from the synthesizer from 1 MHz to 14 GHz and tuned down-conversion frequency of the sampler to become the 1 MHz higher than lower edge of the input signal. The synthesizer and the K6/GALAS were synchronized by an external reference signal. Since the sampled frequency was 2048 MHz, the input signal would rotate 1 million times in 1 s. Then, we performed the Fourier transformed with 2048 points and obtained the millions of phase data.

The phases are shown in Figures 4 and 5. The variation of the phase becomes bigger as input signal became higher frequency. Then, we calculated the standard deviation of each frequency results. It is shown in Figure 2, where we obtain the fitted slope (0.0689 deg/GHz = 0.191 ps) as a jitter. Based on the obtained jitter value. The K6/GALAS is expected a good sampler even the input frequency of 20 GHz.

2.2 Frequency response measurement

K6/GALAS has a capability of receiving signal to K-band. Thus, we measured the frequency response of K6/GALAS precisely. We conducted the measurement in the following way, we input the sine wave from the synthesizer to the K6/GALAS and capture the bit distribution, 3-bits (8-steps). At first we input the 1 GHz signal with -8.5 dBm and recorded the bit distribution as a reference. Then, we input several frequencies up to 20 GHz. As a matter of course, the bit distribution becomes narrow as an input signal becomes higher. We adjusted the power level of the synthesizer to be the same bit distribution as the reference. Note that we measured and corrected the cable loss for the input power. Table 2 shows the result of the bit distribution in each input frequencies. The result of the 22 GHz was within 1-bit level, we input the power level of -3 dBm of 22 GHz separately and re-adjusted the reference distribution. Figure 3 shows the result of the frequency response of K6/GALAS from comparing amplitude from quantized bit distribution between reference signal. Currently, we input the signal from the antenna of 3 to 15 GHz range to the K6/GALAS, and the signal splits lower and higher side of 8 GHz. Thus, a few dB difference should be considered for better observations.

K6/GALAS is produced and maintained by ELECS Industry co.,ltd. `http://www.elecs.co.jp/ElecsIndustry/download/index.html#giga-sampler`

Table 1. Specfications of direct sampler K6/GALAS

Frequency range	0.01 to 24 GHz
Number of analog input	2 (optionally 4)
Sampling rate	16384 or 12800 MHz
Quantization	3 bit
DBBC	1GHz bandwidth, 2 bit, 4 streams
10GbE protocol	VDIF / VTP/ UDP / IP

Table 2. Measured the bit distribution of K6/GALAS as the frequency input from the synthesizer. Since the result of 22 GHz becomes within the 1-bit level, we measured separately.

CW[GHz]	bit step [%]							
	0	1	2	3	4	5	6	7
1, reference	0	25	12	14	12	11	26	0
4	0	18	17	17	15	16	17	0
6	0	13	20	18	16	19	14	0
7	0	7	25	19	17	22	10	0
8	0	0	29	21	19	31	0	0
9	0	1	30	20	17	29	3	0
10	0	1	30	19	17	31	2	0
12	0	0	20	32	28	20	0	0
16	0	0	15	36	36	13	0	0
20	0	0	0	49	51	0	0	0

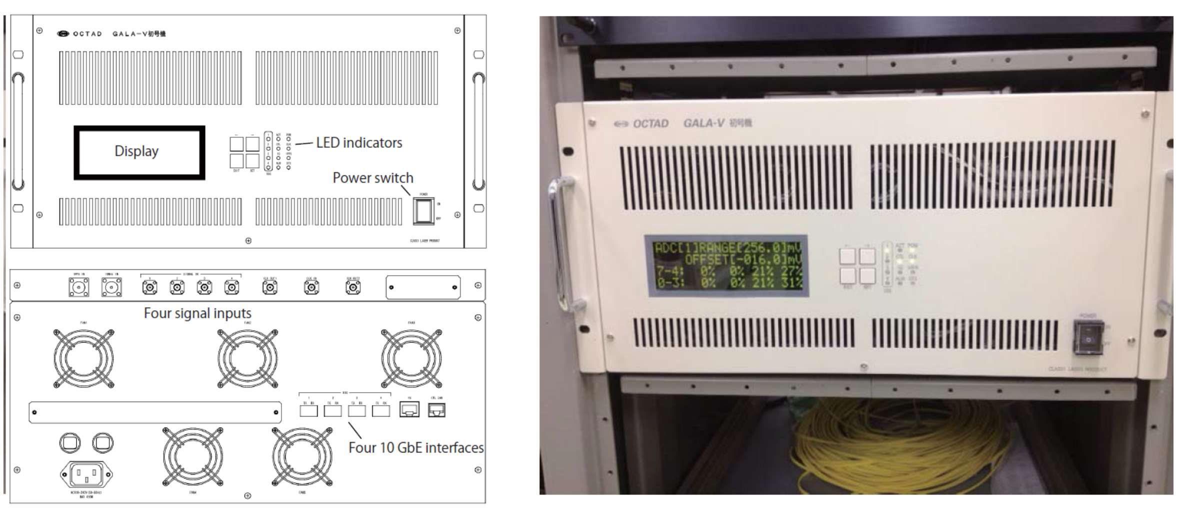

Figure 1. The design of the direct sampler Galas and its appearance.

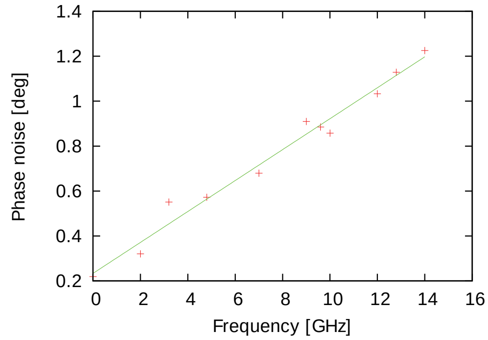

Figure 2. The jitter performance of the direct sampler Galas

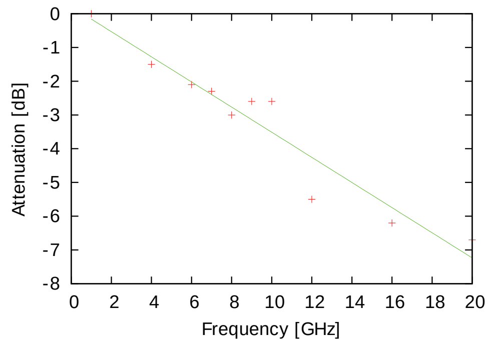

Figure 3. The frequency response of the direct sampler Galas

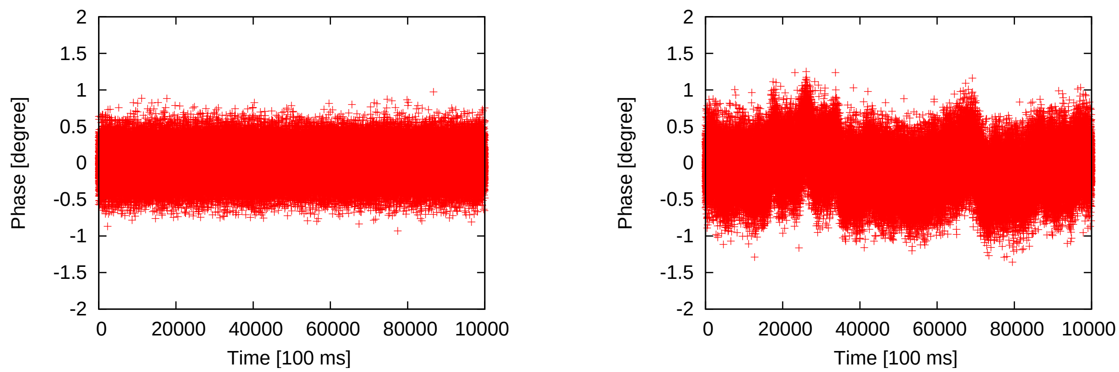

Figure 4. Time-series of the phase, left shows the 1 MHz and right shows the 2GHz input.

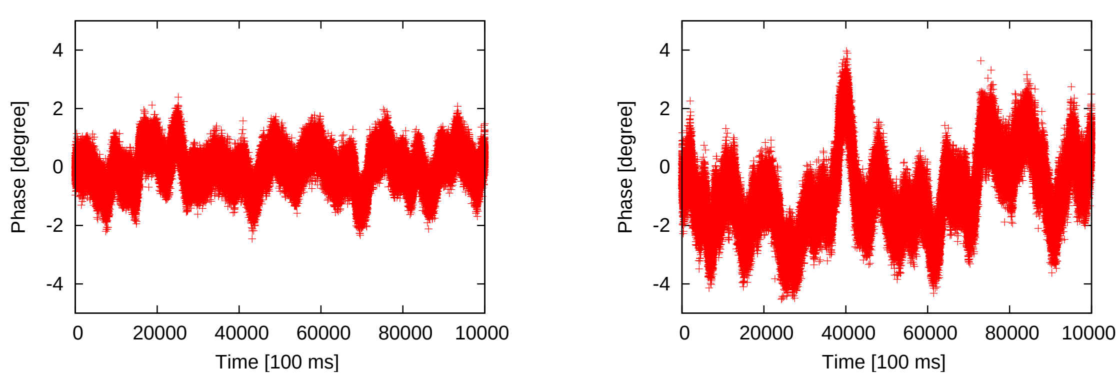

Figure 5. Time-series of the phase measurement, left shows the 7 GHz and right shows the 12 GHz input.

VERICA, A New Verification Method of Applied Calibrations onto Visibility Data (II)

Makoto Miyoshi (*makoto.miyoshi@nao.ac.jp*)

National Astronomical Observatory Japan,
2-21-1 Osawa, Mitaka Tokyo, Japan 181-8588

Abstract In the NICT TDC Symposium in 2014, we introduced a method of verification of data calibration by checking differential visibility between IF channels (Miyoshi 2014) [1]. Raw visibility data includes structure information of the observed source, an independently fluctuating thermal noise, and a systematic error. Data calibration is performed in order to eliminate the systematic error in the visibility. After calibrating the individual recording channels independently, if the systematic error remains partly, the residual systematic error is independent for each channel. When the signal-to-thermal noise ratio is small, it is often in such a state. By creating differential visibility between independently calibrated recording channels, the information of the source structure is common, so they are erased, and what lie there are the difference between the thermal noises and the difference of the residual system errors. If the behavior is different from that of the thermal noise expected from the sensitivity of the baseline, there will be residual systematic errors in the visibility data after the calibration is performed. Here, we show examples in which residual system errors can be found in calibrated data using this method, VERICA (**veri** fication method of **ca** librations onto visibility data), and demonstrate the generality of the VERICA method.

1. Cases of residual systematic errors found by the VERICA methods

In Miyoshi 2014 [1], we showed the examples that has no residual systematic error in the calibrated data of Miyoshi et al. 2011 [2]. From the same data set, this time we show the cases residual systematic errors are still contained in the calibrated data in Figure 1. There are 8 of subsets: (a), (b), (c), & (d) are examples from differential amplitude between IF channels, while (e), (f), (g), & (h) are those from differential phase. Distributions shown in Figure 1 have different features from thermal noise ones, suggesting that some residual systematic errors still exist after the calibration.

There are three types of distributions that seem to contain residual systematic errors. The first cases are existences of outliers largely deviated from estimated distributions of differential thermal noise. Both the subsets (a) & (e) are cases of quite higher signal to noise ratios than 7 (in 10 seconds integration). Almost of the sampled data are fitted well to only thermal noise distributions, but there are outliers as indicated by arrows. In the case of (e), the χ^2 value is more than 6×10^{10} due to the outliers.

The second cases show non-zero-mean distributions of differential visibility. If the errors are thermal noises only, the mean of differential visibility distribution must be zero. While the subsets, (b) and (f) show deviations towards left side from zero as a whole, clearly this is due that one of the IF channels have not a proper, constant offset in calibration solutions.

Single peak at zero is other feature of the distributions of differential visibility containing only thermal noises. (The unique exception is the distributions of differential phases with "no signal": In this case, the distribution shows not a peak but a constant value.) The last cases show not a single peak at zero but multiple peaks. The subsets of (c), (d), (g), & (h) belong to the last cases. The subset (c) shows that multiple peaks distributed in a wide range and that the maximum peak position is not at center (at zero). This may be due to the few number of samples ($N_{data} = 109$), but the maximum peak must be located at zero regardless of the signal to noise ratio in differential amplitude distributions. The subset (d) shows comparable twin peaks: one is at zero and the other is at a minus value. The peaks at the minus value presumably due to residual systematic errors. The subsets (g) & (h) also show twin peaks but in these cases, both are located not at zero, suggesting the existence of residual systematic errors.

2. An example of the VERICA application: a case of no signal noise data

Here we show the case of VERICA application to no signal dataset. The calibrated visibility dataset shown here is from Miyoshi et al. (2003) [3]. They simultaneously observed two of SiO maser lines, namely the v= 1 and v=2 (J =1-0) from VY CMa using the VLBA at Q-band. They performed calibrations of visibility data of the two baseband channels independently. The final image and the calibrated visibility after Hybrid mapping showed accordance in closure phase less than 2°. In Figure 2, we show those of three baselines, the shortest baseline LA-PT (237 km), a modest one HN-OV (3886 km), and the longest one MK-SC (8612 km) in the VLBA. The histograms of differential phase in the lower panels show flat distributions that mean the SNRs of the channels equal zero, namely free from maser emissions. Not only these three examples but all differential phases of 45 baselines show flat distributions. While the histograms of differential amplitude in the upper panels show different features from the nature of pure thermal noises with the expected levels. First, the estimated thermal noise from theoretical curve fitting to the histograms are 5±0, 12±0, 23±0 mJy, which are too low noise levels to be explained from the measured system temperatures. Second, there are several outliers in the bins away from zero. Third, all of the three histograms of differential amplitude show asymmetric features having offsets towards minus direction in the x-axis, which cannot be explained by thermal noise. This may be from different noise levels due to the large frequency difference between the channels. One was for receiving the SiO v=1, the J=1-0 transition at 43.1 GHz, the other was for receiving the SiO v=2, the J=1-0 transition at 42.8 GHz. The difference of frequencies was 305 MHz. The receiver might have not a flat band path character. Anyway, investigations of the differential amplitude distributions allow us to judge that the amplitude calibrations of the data were poorly performed and not a few systematic errors remained after the calibration. As for the phase calibrations of the data, it was performed with very high accuracy as well as 2° in closure phase. While as for the amplitude calibrations of the data, there were unknown problems so that not a few residuals of amplitude systematic errors in the calibrated data. Thus, it is demonstrated that the VERICA method is useful especially for confirming the amplitude calibrations.

References

[1] Miyoshi, M., "A new verification method of applied calibrations onto visibility data", in Proceedings of the 13th NICT TDC Symposium, p. 3, Kashima, Japan, June 2014, `http://www2.nict.go.jp/sts/stmg/ivstdc/news_34/pdf/pctdc_news34.pdf`

[2] Miyoshi, M., Shen, Z-Q., Oyama, T., Takahashi, R., Kato Y., *Publ. Astron. Soc. Japan*, **63**, p1093-1116 (2011).

[3] Miyoshi, M., 2003, in Mass-losing pulsating stars and their circumstellar matter. Workshop, May 13-16, 2002, Sendai, Japan, edited by Y. Nakada, M. Honma and M. Seki. Astrophysics and Space Science Library, **283**, Dordrecht: Kluwer Academic Publishers, p. 303 - 306

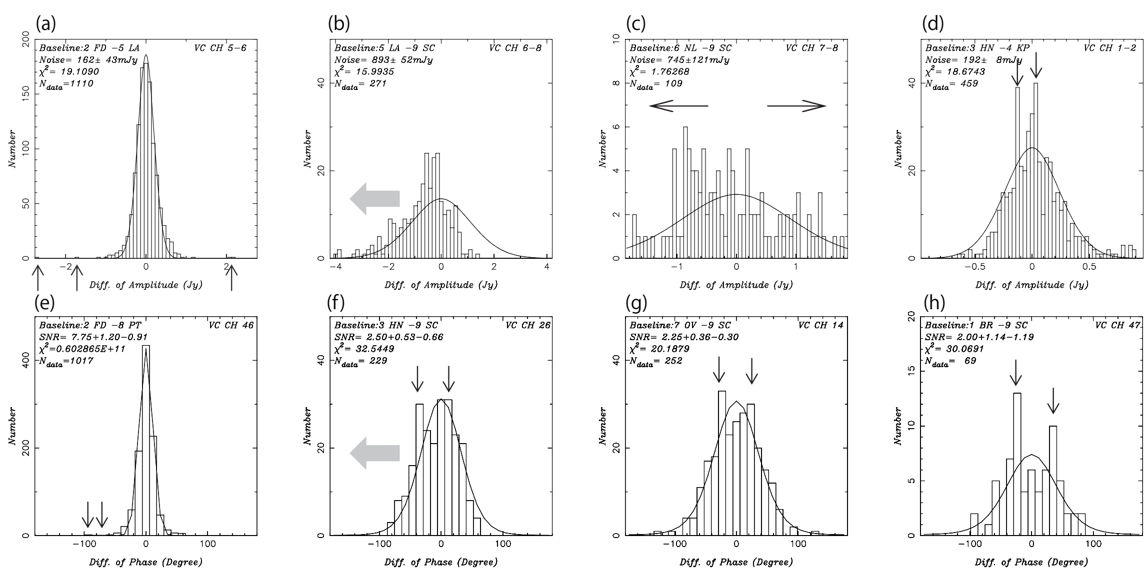

Figure 1. Examples of residual systemic errors found by the VERICA Methods: The cases of differential amplitude distributions are from (a) to (d), and those of differential phase distributions are from (e) to (h). Cases of outliers with a large deviation are (a) and (e). Small vertical arrows indicate outliers. Cases of none zero mean distributions are (b) and (f) which distributions show offsets towards left side (minus direction) as shown by large arrows. The subsets of (c),(d),(g), and (h) show cases of multiple peaks. Also, the subset (f) shows double peaks. These three types of distributions cannot be explained by only the natures of thermal noise, suggesting the existences of residual systematic errors in calibrated data.

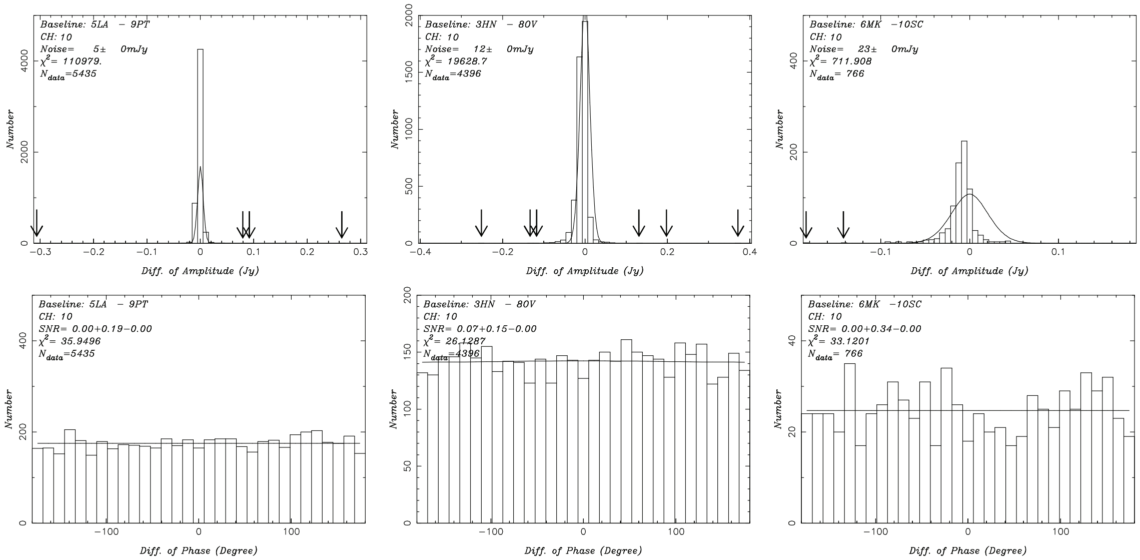

Figure 2. Examples of differential visibility distributions of no signal data: The data are from the 43 GHz VLBA observations of SiO masers from VY CMa (BM099). In order to obtain emissions of the two maser lines (J=1-0 transitions at v=1 and v=2 states) simultaneously, they used two basebands. We picked up velocity channels without maser emissions from the respective two basebands. The upper three panels show histograms in 51-point bins of the distribution of differential visibility amplitude. The arrows in the panels indicate that not a zero value bin exists at the position. The lower three panels show histograms in 31-point bins of the distribution of differential visibility phase. The left two panels show those from LA - PT baseline, the middle two from HN - OV baseline, and the left two from MK-SC baseline. The IF (baseband) channels are between IF 1(sky frequency is 43.1GHz) and IF 2 (sky frequency is 42.8 GHz). The optimized theoretical fitting curve is shown by a solid line. The estimated noise levels are from the least square fitting to differential amplitude distributions (upper panels), The estimated SNRs are from the least square fitting to differential phase distributions (lower panels). The χ^2 *value of the fitting, the number of differential visibility* N_{data} *are shown in every panel. The differential visibility distributions show offsets from zero, and have outliers which suggesting the existences of systematic errors in calibrated data.*

VLBI Direct Sampling Digital Frontend

Kenichi Harada (*harada@elecs.co.jp*),
Yoshinori Hayashi, Kenji Ema,
Yuichi Chikahiro, Hirofumi Onuki,
and Kensuke Ozeki

Elecs Industry Co.,LTd,
1-22-23 Shinsaku, Takatsu, Kawasaki, Kanagawa,
213-0014, Japan

Abstract: We devleloped GIGA SAMPLER and PETA DATA RECORDER for radio astronomy and geodesy. GIGA SAMPLER can directly sample S-band, X-band, and K-band RF analog signal without the IF down converters. Direct sampling eliminate some analog components and reduce system cost and size.

1. GIGA SAMPLER

<Features>

- Wide variation of sampling module from 24Gsps x 3bit to 2Gsps x 12bit.
- Reduce system cost by RF/IF direct sampling up to 24GHz. No need of frequency conversion.
- Signal processing for: Fourier transform, frequency conversion, filter, correlator, demodulation etc.
- FPGA signal processing can be developed by user.
- You can choose integrate type or separate type.
- Optional web-base GUI software made possible the integrative control of signal analysis solution, such as PETA DATA RECORDER and GIGA SAMPLER, via web browser.

<Specifications>

■ ADC module

- 2Gsps x 12bit BW 3GHz (Option BW 18GHz)
- 4Gsps x 10bit BW 10GHz (Option BW 18GHz)
- 24Gsps x 3bit BW 24GHz

■ DSP module

- Fourier transform with window function
- Frequency conversion and filter (Digital Baseband Converter)
- Correlator (auto / cross / delay compensation / fringe rotation / fractional delay [ΔW])
- User custom logic

■ Data output

- 1/10/40Gbit Ethernet
- VTP / VDIF / UDP(TCP) / IP
- Jumbo frame

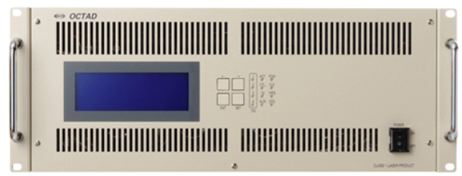

Figure 1. Direct Sampler (integrate type)

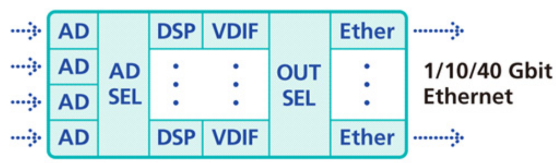

Figure 2. Block Diagram (integrate type)

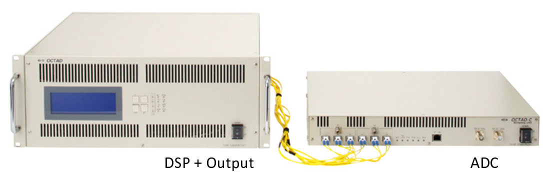

Figure 3. Direct Sampler (separate type)

2. Direct Sampling Benefits

3. PETA DATA RECORDER

<Features>

- Record high-speed and broadband data stream input via 10/40/100G ethernet at maximum speed of 32Gbps.
- Removable storage is safety transported with its own purpose-built carry case.
- The durability of the storage module connector is over 10,000 times of insert / remove.
- Realizing direct analysis of data stream without file format conversion by adopting Linux file system for the storage.
- Optional web-base GUI software made possible the integrative control of signal analysis solution, such as PETA DATA RECORDER and GIGA SAMPLER, via web browser.

<Specifications>

■ Record / Playback

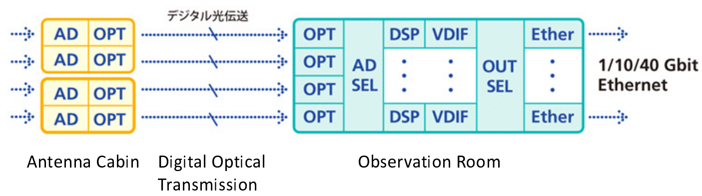

Figure 4. Block Diagram (separate type)

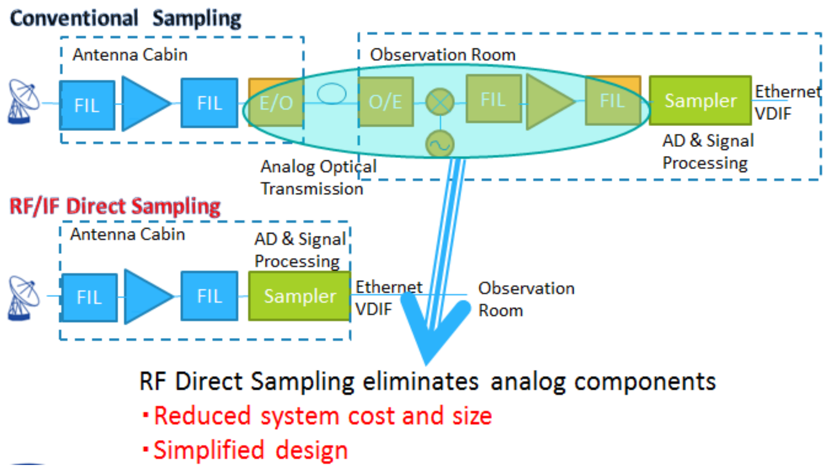

Figure 5. Direct Sampling Benefits

- Maximum Record / Playback speed 32Gbps
- RAID level 0 / 5 / 6
- Linux XFS File system

■ Storage

- Maximum 4 removable storage modules
- 12 HDD/SSD units per 1storage module
- Secured transportation with the own purpose-built carry case

■ Data input / output

- 10/40/100Gbit Ethernet
- Compatible with a wide variety of stream protocol

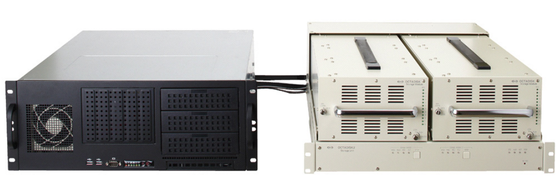

Figure 6. PETA DATA RECORDER

4. Web-baes Integrate GUI Software

<Features>

- Web-base integrate GUI software (GIGA SAMPLER , PETA DATA RECORDER , etc.)
- Don't depend on OS and machine.
- Analyze recorded data (spectrum, quantization bit distribution)
- The control function of other company product can be supported by customization.

5. Delivery Achievement

■ NAOJ (National Astronomical Observatory of Japan)

- VERA (VLBI Exploration of Radio Astrometry)
- Nobeyama Radio Observatory
- Chile Observatory

■ NICT (National Institute of Information and Communications Technology)

- Gala-V (Galapagos VLBI)
- Yamagawa Solar Radio Observatory

■ KASI (Korea Astronomy and Space Science Institute)

Figure 7. Analysis of recorded data

Figure 8. Gala-V Kashima, NICT

Figure 9. KVN Yonsei, KASI

Figure 10. Nobeyama, NAOJ

Figure 11. VERA Mizusawa, NAOJ

Figure 12. Yamagawa, NICT

- KJCC (Korea-Japan Correlation Center)
- KVN (Korean VLBI Network)

■ Ibaraki University

■ Yamaguchi University

“IVS NICT Technology Development Center News” (IVS NICT-TDC News) published by the National Institute of Information and Communications Technology (NICT) (former the Communications Research Laboratory (CRL)) is the continuation of “IVS CRL Technology Development Center News” (IVS CRL-TDC News). (On April 1, 2004, Communications Research Laboratory (CRL) and Telecommunications Advancement Organization of JAPAN (TAO) were reorganized as “National Institute of Information and Communications Technology (NICT)”.)

VLBI Technology Development Center (TDC) at NICT is supposed

1) to develop new observation techniques and new systems for advanced Earth’s rotation observations by VLBI and other space techniques,
2) to promote research in Earth rotation using VLBI,
3) to distribute new VLBI technology,
4) to contribute the standardization of VLBI interface, and
5) to deploy the real-time VLBI technique.

The NICT TDC newsletter (IVS NICT-TDC News) is published biannually by NICT.

This news was edited by Mamoru SEKIDO, Kashima Space Technology Center. Inquires on this issue should be addressed to Mamoru SEKIDO, Kashima Space Technology Center, National Institute of Information and Communications Technology, 893-1 Hirai, Kashima, Ibaraki 314-8501, Japan, e-mail : sekido@nict.go.jp.

Summaries of VLBI and related activities at the National Institute of Information and Communications Technology are on the Web. The URL to view the home page of the Radio Astronomy Applications Section of the Space-Time Measurement Group of Space-Time Standards Laboratory is : **“http://www2.nict.go.jp/sts/stmg/ivstdc/news-index.html”**.

IVS NICT TECHNOLOGY DEVELOPMENT CENTER NEWS No.36, November 2016

International VLBI Service for Geodesy and Astrometry
NICT Technology Development Center News
published by
National Institute of Information and Communications Technology, 4-2-1 Nukui-kita, Koganei, Tokyo 184-8795, Japan